AD-A193 792 SPACE-CHARGE-WAVE SOLID STATE MICROWAVE AMPLIFIER(U) 1/1
AEROJET ELECTROSYSTEMS CO AZUSA CA B G MARTIN
31 DEC 87 ARO-23444.1-PH DAAL03-86-C-0016

UNCLASSIFIED F/G 9/1 NL

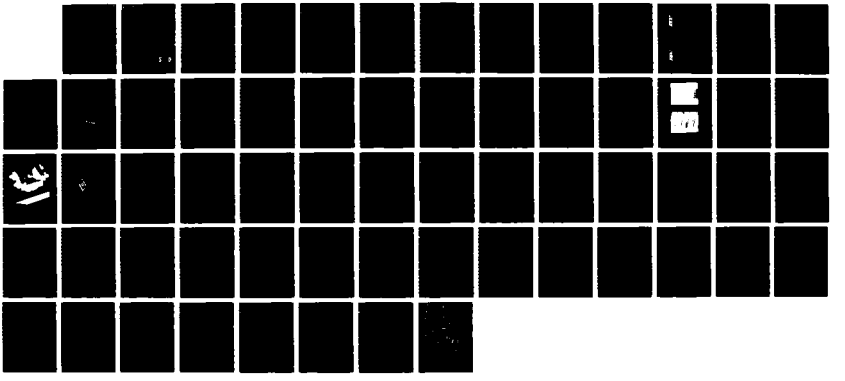

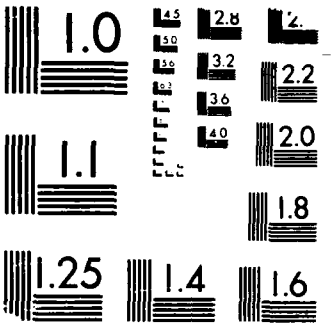

MICROCOPY RESOLUTION TEST CHART

ARO 23444.1-PH (2)

SPACE-CHARGE-WAVE SOLID STATE MICROWAVE AMPLIFIER

Aerojet ElectroSystems Company
1100 West Hollyvale Street
Azusa, CA 91702

31 December 1987

FINAL REPORT

Contract No. DAAL03-86-C-0016

Prepared for

U.S. ARMY RESEARCH OFFICE
P.O. Box 12211
Research Triangle Park, North Carolina 27709-2211

UNCLASSIFIED
SECURITY CLASSIFICATION OF THIS PAGE

MASTER COPY - FOR REPRODUCTION PURPOSES

REPORT DOCUMENTATION PAGE

1a. REPORT SECURITY CLASSIFICATION: Unclassified	1b. RESTRICTIVE MARKINGS
2a. SECURITY CLASSIFICATION AUTHORITY	3. DISTRIBUTION/AVAILABILITY OF REPORT: Approved for public release; distribution unlimited.
2b. DECLASSIFICATION/DOWNGRADING SCHEDULE	
4. PERFORMING ORGANIZATION REPORT NUMBER(S)	5. MONITORING ORGANIZATION REPORT NUMBER(S): ARO 23444.1-PH
6a. NAME OF PERFORMING ORGANIZATION: Aerojet ElectroSystems Co. / 6b. OFFICE SYMBOL (If applicable)	7a. NAME OF MONITORING ORGANIZATION: U. S. Army Research Office
6c. ADDRESS (City, State, and ZIP Code): 1100 West Hollyvale Street, Azusa, CA 91702-3333	7b. ADDRESS (City, State, and ZIP Code): P. O. Box 12211, Research Triangle Park, NC 27709-2211
8a. NAME OF FUNDING/SPONSORING ORGANIZATION: U. S. Army Research Office / 8b. OFFICE SYMBOL (If applicable)	9. PROCUREMENT INSTRUMENT IDENTIFICATION NUMBER: DAAL03-86-C-0016
8c. ADDRESS (City, State, and ZIP Code): P. O. Box 12211, Research Triangle Park, NC 27709-2211	10. SOURCE OF FUNDING NUMBERS: PROGRAM ELEMENT NO / PROJECT NO / TASK NO / WORK UNIT ACCESSION NO

11. TITLE (Include Security Classification)

Space-Charge-Wave Solid State Microwave Amplifier

12. PERSONAL AUTHOR(S)

B. G. Martin

13a. TYPE OF REPORT	13b. TIME COVERED	14. DATE OF REPORT (Year, Month, Day)	15. PAGE COUNT
Final	FROM Sept. '86 TO Oct. '87	1987, Dec. 31	56

16. SUPPLEMENTARY NOTATION

The view, opinions and/or findings contained in this report are those of the author(s) and should not be construed as an official Department of the Army position, policy, or decision, unless so designated by other documentation.

17. COSATI CODES			18. SUBJECT TERMS (Continue on reverse if necessary and identify by block number)
FIELD	GROUP	SUB-GROUP	Microwaves, GaAs HEMT, space charge waves

19. ABSTRACT (Continue on reverse if necessary and identify by block number)

This investigation was on the feasibility of a device utilizing the GaAs/AlGaAs HEMT structure for amplifying microwaves. The following accomplishments were made.

(1) A number of design considerations bearing on concept feasibility were investigated, e.g., carrier scattering losses, LO phonon creation, penetration depth of microwaves into HEMT structure, etc. Based on these considerations, the concept appears feasible.

20. DISTRIBUTION/AVAILABILITY OF ABSTRACT	21. ABSTRACT SECURITY CLASSIFICATION
☐ UNCLASSIFIED/UNLIMITED ☐ SAME AS RPT ☐ DTIC USERS	Unclassified
22a. NAME OF RESPONSIBLE INDIVIDUAL	22b. TELEPHONE (Include Area Code) / 22c. OFFICE SYMBOL

DD FORM 1473, 84 MAR — 83 APR edition may be used until exhausted. All other editions are obsolete.

SECURITY CLASSIFICATION OF THIS PAGE
UNCLASSIFIED

(2) Fabrication techniques were developed for interdigital electrode slow-wave circuits and ohmic contacts on HEMT structures.

(3) Several prototype devices were fabricated and tested. A result of this was that coupling of microwaves (at GHz frequencies) to the HEMT channel electrons was demonstrated.

(4) Theoretical work showed that the TO phonons in doped GaAs behave as the "resistive wall" necessary for electromagnetic wave amplification. In addition, an investigation was made on the interaction of electromagnetic waves and drifting electrons in a model of a HEMT structure. Amplifying instabilities are in evidence.

It is concluded that the subject device appears feasible, but further and extensive experimental work is required.

SPACE-CHARGE-WAVE SOLID STATE MICROWAVE AMPLIFIER

B. G. Martin

Aerojet ElectroSystems Company
1100 West Hollyvale Street
Azusa, CA 91702

31 December 1987

FINAL REPORT

Contract No. DAAL03-86-C-0016

Prepared for

U.S. ARMY RESEARCH OFFICE
P.O. Box 12211
Research Triangle Park, North Carolina 27709-2211

TABLE OF CONTENTS

ACKNOWLEDGEMENTS

The author wishes to express appreciation to Dr. M. Ciftan of the Army Research Office, who was contract monitor for this program, to Mr. M. Muzilla and Mr. B. Gable of Aerojet ElectroSystems, who did the MBE growth of the material and fabricated the devices, and to Mr. I. Galin of Aerojet ElectroSystems, who made the microwave measurements.

I also wish to thank Dr. C. K. Birdsall of UC Berkeley, who was a consultant for the microwave measurement portion of the program.

Finally, I want to thank Dr. R. F. Wallis of the University of California, Irvine, for collaboration on much of the theoretical work as well as for many helpful discussions.

SPACE-CHARGE-WAVE SOLID STATE MICROWAVE AMPLIFIER

I. INTRODUCTION

The overall objective of this program was to investigate the feasibility of a solid-state microwave amplifier based on SCW interactions in GaAs/AlGaAs modulation doped heterostructures or HEMT's, specifically the resistive-wall analog discussed below.

Specifically, the program objectives were to (1) investigate the growth and characterization of HEMT structures, (2) fabricate a slow-wave structure for coupling microwaves to the electron stream, (3) determine whether or not the coupling took place, and (4) explore theoretical design and experimental approaches that would bear on amplifier feasibility.

During the last two decades or so there has been interest in exploring solid state plasmas for the various types of instabilities observed in gaseous plasmas[1-9]. In the latter, for example, there are so-called resistive-wall space-charge-wave instabilities[10,11] which have been used for amplifying microwaves. Such instabilities also occur in solid state plasmas[12-22].

Consider a metal or doped semiconductor, i.e., a solid state plasma. Space charge waves (SCWs) are set up when a dc electric field is imposed and the free charge carriers, electrons say, are being modulated by an ac electromagnetic field. An electron stream is created that has a drift velocity proportional to, and in the direction of, the dc field. The ac modulating field causes variations in the electron number density and, as a consequence, creates SCWs. They arise in pairs, one wave having a phase velocity greater than, and the other having a phase velocity less than, the electron drift velocity. The velocity difference depends on the plasma frequency and system geometry. Specifically, the wave vectors, $\pm K$, of the SCWs are given by[23]

$$K_{\pm} = \frac{\omega \pm F\omega_p}{V_o} \tag{1.1}$$

where ω is the modulation frequency, ω_p is the plasma frequency, and V_o is the drift velocity. The factor F depends on geometry, e.g., for a plane surface bounding a semi-infinite solid, F = 1. The (+) and (-) signs correspond to the slow and fast SCWs, respectively.

To gain an understanding of the energies involved, consider an observer moving to the right at the electron drift velocity. He sees that the slow SCW moves with negative phase velocity, i.e., it travels to the left while the fast SCW has positive phase velocity and thus moves to the right. Consequently, one can think of the slow space-charge-wave as having negative energy[24]. These considerations let Chu[25] to

postulate, for the interaction of SCWs in contact with a resistive medium, the amplification of the slow SCWs. This has been termed resistive-wall amplification. Subsequently, using a gas plasma, Birdsall et al.[10] fabricated a working microwave amplifier based on Chu's idea. In addition, amplification can take place from the interaction of SCW's associated with two electron streams. Here, when the phase velocity of the fast SCW of one stream is equal to, or greater than, the phase velocity of the slow SCW of the second stream, amplification of the latter takes place. Gas plasma microwave amplifiers have been analyzed and constructed[26-28] based on this interaction and are usually called two-stream amplifiers. An analysis of one solid-state analog of the two-stream amplifier is given in Ref. 14.

Additional theoretical work has been done on instabilities associated with the interaction of electromagnetic waves and drifting carriers. Under suitable conditions, surface polaritons can be made to propagate along the surface of a semiconductor containing free carriers. If a dc electric field is applied so that a drift current flows parallel to the surface, instabilities of the surface polariton may arise. A surface polariton is an electromagnetic wave that propagates along the interface between two media, its basic properties being obtained by solving Maxwell"s equations. Surface polariton dispersion theory provides the most fundamental approach for investigating surface wave instabilities, and is one that has not been extensively used in the past.

A theoretical investigation has been made[29] of such instabilities for the case of n-type silicon with the current parallel to the propagation direction of the surface polariton. The dispersion relation for surface polaritons was derived using the specular reflection approach of Kliewer and Fuchs.[30] Surface polariton modes with a growing wave character were found for both a silicon-vacuum interface and a silicon-dissipative medium interface. For the former, which took into account carrier damping,the growing wave is an evanescent wave (non-amplifying) in the terminology of Sturrock[31], while the latter is a convective instability, i.e., an amplifying wave. The dissipative medium was modeled by replacing the vacuum layer ($\varepsilon_m = 1$) by one where $\varepsilon_m = \varepsilon_1 + i\,\varepsilon_2$, with $\varepsilon_2 = 4\pi\sigma/\omega$, where σ is the dc conductivity.

Additional work[29] was concerned with two semiconductor media where each one is represented by the same form of the dielectric tensor, but can differ in medium parameters, such as background dielectric constant, plasma frequency, and drift velocity. Dispersion calculations were done taking into account retardation and carrier damping.

It was found that for carriers drifting in the same direction, surface SCW interaction gives rise to convective instabilities. For carriers drifting in the opposite direction, however, the surface wave interaction gives rise to a non-convective instability, i.e., one that is not amplifying.

Subsequent to the theoretical work described above, a GaAs-AlGaAs HEMT/inverted HEMT design for exploiting SCW amplifying instabilities was devised*. Figure 1 shows the generalized amplifier design and a HEMT/inverted HEMT structure that provides electron populations with different mobilities. This design is a solid state analog of the gas plasma two-stream amplifier.

The choice of the HEMT/inverted HEMT structure was based on the following considerations, among others:

a. The electron mobility should be as high as possible to minimize the problem of coupling the electromagnetic wave to the drifting electrons.

b. The amplifier gain is proportional to the electron plasma frequency; thus the electron concentration should be such that the plasma frequency and the microwave frequency of interest should be nearly equal.

c. The two electron streams should be close enough to each other so that the SCWs of each overlap. This is, of course, necessary because it is the interaction of SCWs which causes amplification.

Using molecular beam epitaxy, it is possible to grow heterojunction structures whereby the free electrons can be separated from the vicinity of their donors, thus minimizing ionized impurity scattering and achieving high electron mobility. Electrons originating from donors in the $Al_xGa_{1-x}As$ layer of the HEMT structure (see Fig. 1) are transferred to the undoped GaAs layer. The space charge that results creates a strong electric field (over 10^5 volts/cm) that causes the formation of a triangular potential well. In addition, aided by the bandgap discontinuity (see Fig. 2), the electrons are confined to the interface region and are thus spatially separated from the donors. There is an electron concentration of $\sim 10^{18} cm^{-3}$ in the channel whose width is ~ 50A. Thus, essentially one has a two-dimensional electron gas.

The near absence of ionized impurity scattering changes the temperature dependence of mobility such that as the temperature decreases, the mobility increases up to a point. Other scattering processes are (1) Coulombic interaction between the donors and free electrons, and (2) the scattering from background ionized impurities in the GaAs layers. Results on MBE grown GaAs indicate that the background ionized carrier concentration is of the order of 10^{14} cm^{-3} range(32). However, it appears that the high mobility electrons effectively screen the background ionized impurities(33).

The Coulombic interaction between donors and conduction electrons across the interface can be reduced by using a thin, undoped Al_xGa_{1-x} As layer between the doped $Al_xGa_{1-x}As$ layer and the undoped GaAs layer, as shown in Figure 1.

*A patent disclosure has been submitted for this design.

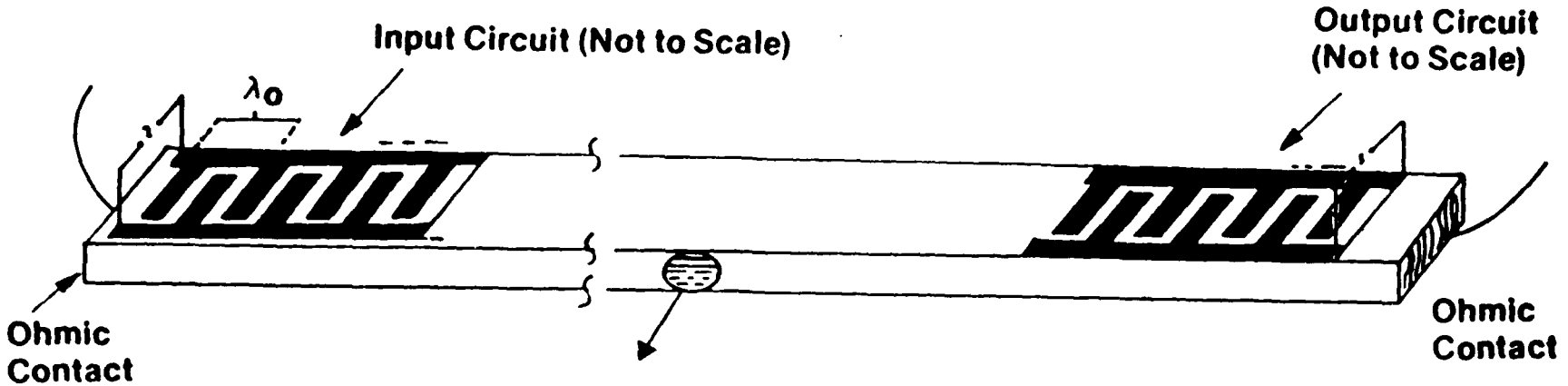

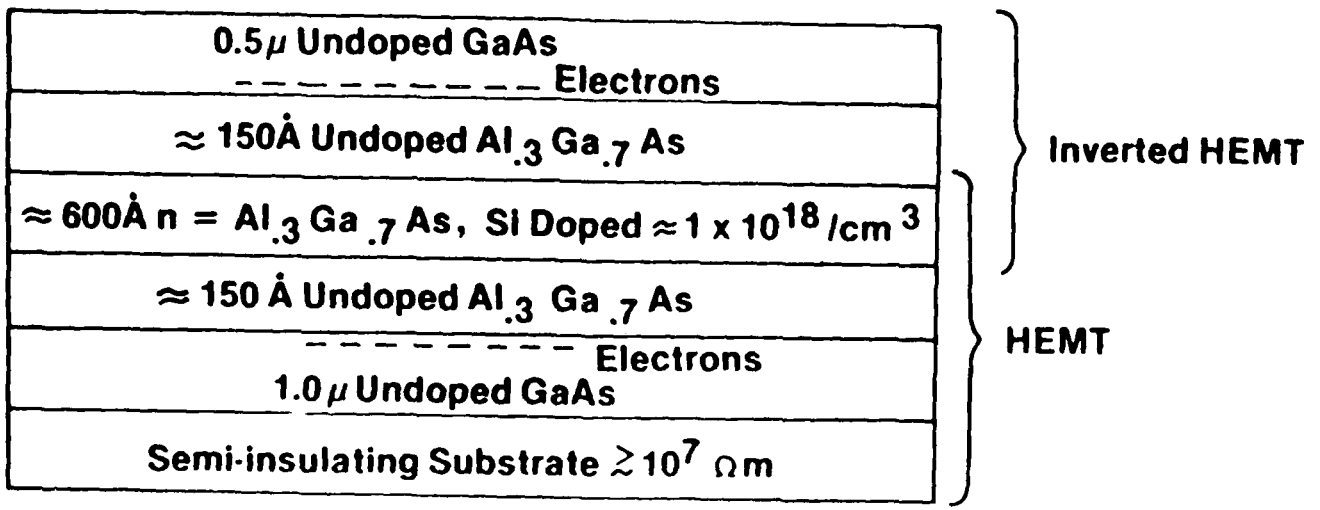

Figure 1. Space-Charge-Wave (SCW) Solid State Microwave Amplifier

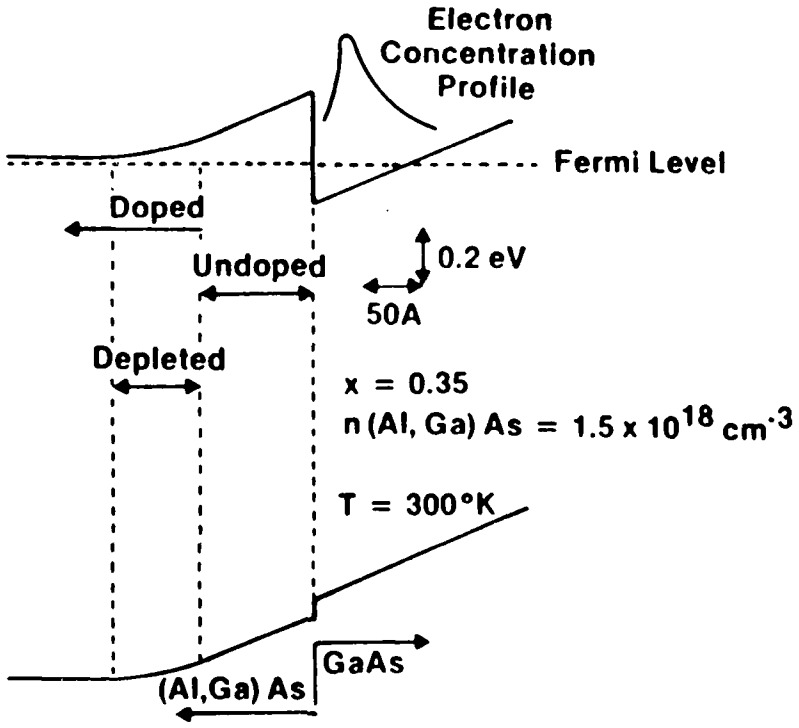

Figure 2. Band Diagram (Drawn to Scale) Of A Single Period Al_x Ga_{1-x} As/GaAs Modulation Doped Heterostructure Having An Undoped $Al_xGa_{1-x}As$ Spacer Layer Thickness Of 100A

The difference in channel electron mobilities in the HEMT vs. inverted HEMT structure is a result of the different properties of GaAs grown prior to, and after the $Al_xGa_{1-x}As$ growth. The situation when GaAs is grown on (Al,Ga)As (inv. HEMT layers) is different from that of the HEMT structure[34]. This results in a lower electron mobility, estimated to be lower by a factor of 2-5.

However, during the course of this investigation, experimental work was done only on the inverted HEMT structure (see Fig. 1).

In what follows, amplifier design considerations are discussed in Section 2, device growth and characterization in Section 3, design and fabrication of ohmic contacts and the slow-wave circuit in Section 4, amplifier testing in Section 5, and theory in Section 6. Conclusions are presented in Section 7.

2 Amplifier Design Considerations

There are many factors to consider in determining the best design for the solid state analogs, namely the resistive-wall amplifier and the dual-stream amplifier. Given below is a general, somewhat qualitative discussion of design parameters that bear on the feasibility and practicality of a solid-state amplifier.

2.1 General Consideration

Of primary interest is the gain available from a GaAs/AlGaAs HEMT or HEMT/inverted HEMT structure. The gain of an amplifier based on SCW interactions in the HEMT/inverted HEMT structure is proportional to the distance traveled by drifting carriers[29]. These structures would be grown using MBE and, at present, this limits the length to approximately 5 cm.

The gain is maximum at near the plasma frequency, which is proportional to the square root of the carrier concentration. For a typical GaAs/AlGaAs HEMT structure, as discussed earlier, the electron "channel" density is $\sim 10^{11}$ cm^{-2}. The channel width is ~50A so that the electron concentration is $\sim 2 \times 10^{17}$ cm^{-3}. This corresponds to a plasma frequency $\omega_e \sim 3 \times 10^{13}$ sec^{-1}, which is in the infrared region and is much higher than the microwave frequencies of interest here, namely 10^{10}-10^{11} sec^{-1}. However, the HEMT channel electron concentration can be controlled by the spacer-layer thickness (see Figure 1) and gate electric field (Ref 35), where, for our situation, the interdigital electrode acts as a gate. Figure 3 shows the current-voltage characteristic curve for an Aerojet-grown HEMT device. In addition to controlling the channel electron concentration, the extent of the depletion region of the Si-doped AlGaAs can be controlled by the gate bias and/or by the layer thickness. Further discussion of this point will be given below in Section 2.2.

The carrier concentrations in the HEMT structure are many orders of magnitude higher than they are in a gas plasma microwave amplifier. Consequently, much higher gain is expected.

The mobility in a GaAs/AlGaAs HEMT is of the order of 10^5 - 10^6 cm^2/volt-sec[36], and that of the inverted HEMT smaller by a factor of 2-5, as mentioned above. At a temperature of 4.2°K, the electron mobility limit is estimated to be $\sim 9 \times 10^6$ cm^2/volt-sec[37]. The electron peak or saturation drift velocity is $\sim 2 \times 10^7$ cm/sec at 300°K and $\sim 3 \times 10^7$ cm/sec at 77°K, the latter probably not increasing substantially even at 4.2°K. The operating temperature of the proposed device would be 77°K. The fact that the magnitude of the mobility and the peak drift velocity are close to each other means that the dc bias field need not be large to attain the maximum drift velocity.

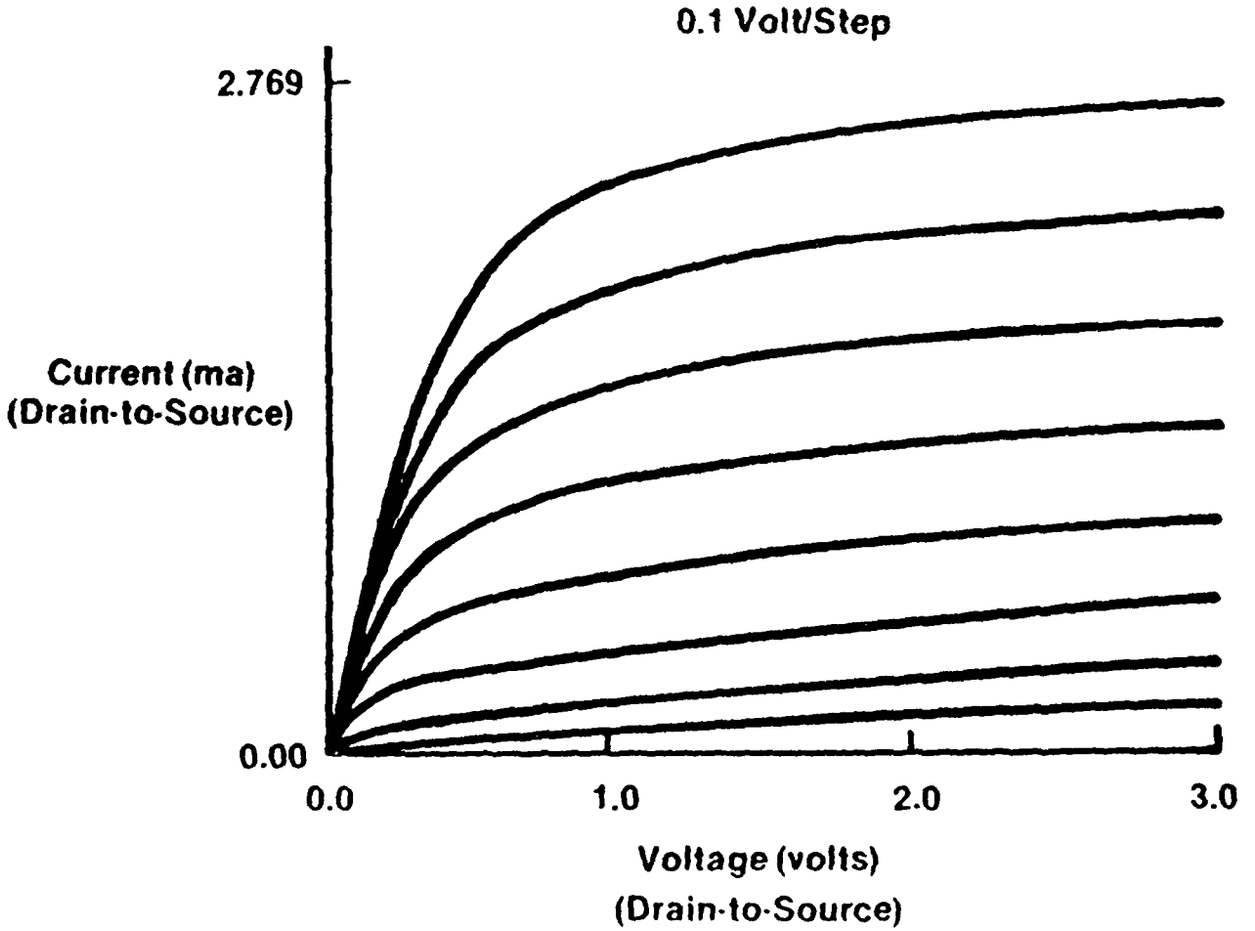

Figure 3. I-V Characteristic Curve For Aerojet H.E.M.T. Device

To amplify microwaves in the proposed device, there must be a near match of the electromagnetic wave phase velocity and the carrier drift velocity. This assures efficient coupling. A major problem in utilizing a solid state analog of the gas-plasma amplifier is the coupling. For a gas plasma, the electron drift velocity can be within a factor of 10 of the vacuum electromagnetic wave phase velocity. In a solid state plasma, on the other hand, the carrier drift velocity is at most ~10^7 cm/sec, (as has been discussed), a factor of ~10^3 less than that of the electromagnetic wave. In other words, in order to achieve resonant interaction with charge carriers, the electromagnetic wave phase velocity must be reduced by at least three orders of magnitude. What is required to do this is a so-called slow-wave circuit, examples of which are helix and interdigital electrode structures. A third slow-wave circuit is the meander line. Designing and fabricating an efficient slow-wave circuit for the solid state plasma is a major task and is discussed below. If the dc voltage gradient is large for a slow-wave circuit, special insulation problems may appear. As a consequence, it is desirable to have the dc voltages as small as possible[38], a virtue the HEMT structure has, as mentioned above.

In a HEMT structure, the electrons are in a channel which takes them away from the ionized donors from which they originated. Thus, scattering is reduced and as a consequence, there is very high mobility. In other words, the scattering or collision time, τ, is longer than in conventional doped semiconductors. Solymar and Ash[16] state that, for gas plasmas, one has that $\omega\tau >> 1$ and that the drift velocity, V_D, is large compared with the random thermal velocity, i.e., $V_D > V_T$. If these conditions occur in a solid state plasma, then the differences between a solid state plasma and gas plasma or vacuum electronics are small. First consider the electron scattering time associated with the GaAs/AlGaAs HEMT structure. One can obtain an estimate of τ from the general mobility expression

$$\mu = \frac{e}{m^*} \left(i\omega + \frac{1}{\tau}\right)^{-1} \tag{2.1}$$

Using the values $m^* = 0.067\ m_o$ and $\mu = 10^6$ cm^2/volt-sec*, we obtain for ω = 10 GHz, the result $\omega\tau \sim 1$. This indicates that, for the microwave frequency regime of interest, collision losses are small compared with the conventional solid-state plasma where $\omega\tau << 1$.

Although, in a HEMT device, the channel electrons are essentially removed from ionized impurity scattering, polar mode scattering can occur[39,40]. The threshold energy for longitudinal optical phonon emission is 0.035 eV. For energies equal to or above this value, the electrons will lose up to 0.16 eV/psec during their transit time[40]. The highest electron drift velocity that can be attained before spontaneous phonon emission is given by the expression

*This value of μ is higher than has yet been achieved in inverted HEMT structures grown at Aerojet.

$$\frac{1}{2} m_e^* v_D^2 = h\omega_{LO} , \tag{2.2}$$

where m_e^* is the electron effective mass, v_D is the drift velocity, and ω_{LO} is the longitudinal optical phonon frequency. Putting in appropriate values in Eq. (2.2) gives the result $v_D \simeq 3 \times 10^7$ cm/sec. This can therefore be considered an upper limit on drift velocity and consequently applied bias. This is the drift saturation velocity at T=77°K, as discussed above.

Consider next the mean thermal velocity for GaAs. The thermal velocity is given by

$$V_T = \left(\frac{K_B T}{m_e^*} \right)^{1/2} \tag{2.3}$$

and we find that for 300°K and 77°K, respectively, $V_T = 3 \times 10^7$ cm/sec and 1×10^7 cm/sec. This is comparable to the maximum obtainable drift velocity, V_D, i.e., $V_T \sim V_D$. In a conventional doped semiconductor, $V_D << V_T$. A requirement on device feasibility is that the random thermal energy be less than the energy corresponding to electron drift.

From the above considerations, we see that with the HEMT structure, one is nearer the situation that exists in a gas plasma that is the case for a conventional doped semiconductor.

2.2 Resistive-Wall Analog

Here we present the solid-state analog of the resistive-wall amplifier (see Ref. 10). It was this type of device that was used to make the microwave measurements discussed in Section V.

Consider electrons in a channel with adjacent resistive walls. The appropriate dispersion relation for one interactive interface is, in the non-retarded limit,

$$\frac{\varepsilon_\infty}{\varepsilon_d} \left[1 - \frac{\omega_p^2}{(\omega - k V_o)^2} \right] = -1, \tag{2.4}$$

where ε_∞ is the background dielectric constant for the channel material (GaAs), and ε_d is the dielectric constant for the adjacent, resistive half-space which can be taken in the form

$$\varepsilon_d = \varepsilon_\infty + i\frac{4\pi\sigma}{\omega}, \tag{2.5}$$

where σ is the conductivity. In expression (2.4), k is wave vector and V_o is the carrier drift velocity. In writing Eq. (2.5), we have assumed that the fields vary as exp [i(ky-ωt)], taking y as the propagation direction.

In Eq. (2.4) carrier damping has been neglected, while in medium ε_d the carrier drift velocity relative to that in the channel has been neglected. In what follows, we take $\varepsilon_\infty = \varepsilon_r = 13.1$ (GaAs).

Substituting Eq. (2.5) into Eq. (2.4) and solving for wave vector k gives the result

$$\frac{V_o k}{\omega_p} = \frac{\omega}{\omega_p} \pm \left[\frac{\varepsilon_\infty \frac{\omega}{\omega_p}\left(2\varepsilon_\infty - i\frac{4\pi\sigma}{\omega_p}\right)}{4\varepsilon_\infty^2 + \left(\frac{4\pi\sigma}{\omega_p}\right)^2} \right]^{1/2}, \tag{2.6}$$

Now to calculate values of $V_o k/\omega_p$, we need values for ω_p, the channel plasma frequency, and σ, the conductivity of the resistive wall (which we take as doped AlGaAs).

In a HEMT structure channel, $n = 10^{11}$ cm^{-2} (GaAs HEMT). The electron channel is approximately 50Å wide so that the electron concentration $n_e = 2 \times 10^{17}$ cm^{-3}. For GaAs, $\varepsilon_x = 13.1$ and $m_e^* = 0.067\ m_o$ so that

$$\omega_p^2 = \frac{4\pi n_e q^2}{\varepsilon_x m_e^*} \simeq 7.25 \times 10^{26}, \tag{2.7}$$

or $\omega_p \simeq 2.7 \times 10^{13}$ sec^{-1}.

If the AlGaAs layer is totally depleted, its conductivity would be that of undoped GaAs, namely

$$\sigma = 2.7 \times 10^3\ sec^{-1}. \tag{2.8}$$

Consider Eq. (2.6) again. The square bracketed term is complex because of the presence of the imaginary part, i.e., i $4\pi\sigma/\omega_p$. Thus Eq. (2.6) can be written as

$$k = k_r \pm ik_i, \tag{2.9}$$

from which we see that the negative sign would give a wave that is amplifying while the positive sign gives an exponentially decaying wave.

If the resistive wall is of undoped GaAs, one finds using the values given in (2.7) and (2.8) above that $4\pi\sigma/\omega_p \simeq 4\pi \times 10^{-10} \simeq 0$, relative to the real quantities in Eq. (2.6). Therefore, essentially no electromagnetic wave amplification would take place. To have amplification, σ and ω_p should be of like magnitude. If the AlGaAs layer is not totally depleted of carriers, then the AlGaAs conductivity may be sufficient to provide measurable amplification.

Thus to ensure a high enough value of conductivity in the Si-doped AlGaAs layer, one would choose the thickness such that it wouldn't be depleted or, make use of a gate bias as discussed above.

2.3 Dual-Stream Analog

The two-stream amplifier discussed here differs in a fundamental way from traveling wave tubes. As will be discussed below, electromagnetic circuits are required to impress a signal on the electron stream, and to produce an electromagnetic output by means of the amplified signal present in the slow SCW. The amplification of microwaves, however, takes place in the electron flow itself, and increases as it travels. Amplifiers based on this principle have several advantages. Because the electrons, or rather the SCWs associated with them, interact with one another, the electron stream does not need to pass extremely close to the electromagnetic circuit elements. In addition, if the distance of electron flow between input and output circuits is long enough, amplification can take place even if the input and output circuits have very low impedance or poor coupling to the electron streams[26]. Even though the region of amplification is the distance between input and output circuits, there is no need to maintain a close synchronism between the electron velocity and electromagnetic wave velocity, as is the case in the usual traveling wave tube[26].

To our knowledge, no one has built a solid-state, two-stream amplifier and consequently no actual gain results have been obtained. However, some gain measurements have been made for two-stream, gas plasma microwave amplifiers[26,28]. Hollenberg[28] obtained a gain of 33 dB at a center frequency of 0.255 GHz. Haeff[26] observed electronic gains at the order of 80 dB at a frequency at 3 GHz.

There are a number of other design considerations, e.g., the penetration depth of the electromagnetic wave, the interaction distance between the two drifting electron populations, and the dielectric relaxation of SCWs.

For the dual stream device, a major question is whether or not the electromagnetic waves in the slow-wave structure penetrate deep enough to encompass both electron streams. This penetration depth can be estimated as follows. Let $v_{p_o} = 3 \times 10^7$ cm/sec be the electromagnetic phase velocity in the slow-wave structure (see Figure 1). In GaAs, the phase velocity, v_p, will be

$$v_p = \frac{v_{p_o}}{\sqrt{\varepsilon_\infty}} = 8.7 \times 10^6 \, cm/sec \tag{2.10}$$

Taking z to label the direction normal to the layers, the associated wave vector, k_z, is

$$k_z = \frac{\omega}{v_p} = 0.72 \times 10^{-6} f, \tag{2.11}$$

where f is frequency. The penetration depth is determined by exp ($-k_z d$), where d is the distance as measured from the surface. Taking d = 6 x 10^{-5} cm (see Fig. 1), one finds that for f = 1 GHz, exp ($-k_z d$) = 0.96, while for f = 10 GHz, exp ($-k_z d$) = 0.65. Thus, in this frequency range at least, the microwaves would penetrate deep enough to encompass both electron streams.

The dielectric relaxation frequency, ω_p, gives the damping rate of SCW's:

$$\omega_p = \sigma/\varepsilon = \frac{1}{p\varepsilon} \tag{2.12}$$

The question of dielectric relaxation losses is different for two-stream SCWs than it is for single-stream SCWs[39]. Mizushima and Sudo[14] state that ω_p should be comparable to the signal frequency, ω, which in our case is in the 10-100 GHz regime. More specifically, they state that[14]

$$\frac{\omega_p}{\omega} > \frac{\omega}{\omega_D}, \tag{2.13}$$

where ω_D is the diffusion frequency, namely $\omega_D = eV_D^2/k_B T\mu$. The above inequality is equivalent to saying that the magnitude of the SCW wave vector in the carrier propagation direction is greater than the wave vector magnitude in the transverse direction. It appears that the pertinent variables for the GaAs/AlGaAs HEMT structure and the operating temperature can be modified to satisfy this inequality.

A question that comes to mind is whether or not the proposed amplifier design can be improved upon by increasing the number of electron channels. This question was considered within the context of gas plasma amplifiers where it was shown[41-43] that gain is optimum only when two distinct drift velocities are present.

Another consideration is the noise to be expected from a solid state, two stream microwave amplifier. Haeff[26] has stated for the two-stream, gas-plasma microwave amplifier that the signal-to-noise ratio was expected to approach that of a conventional triode of that year (1949). Noise problems associated with the proposed amplifier have yet to be determined.

III. GROWTH AND CHARACTERIZATION OF HEMT/INVERTED HEMT STRUCTURE

3.1 Materials Growth

The inverted HEMT structures were grown by Molecular Beam Epitaxy (MBE). Aerojet has demonstrated high two-dimensional electron gas (2 DEG) mobilities in conventional HEMT structures. For undoped $Al_xGa_{1-x}As$ spacer layers 140 A thick, 2 DEG mobilities in excess of 135,000 cm^2/volt-sec at 77°K have been achieved reproduceably. The inverted structures have, possibly due to interface roughness, mobilities which are a factor of 2 to 5 lower than the conventional (i.e., $Al_xGa_{1-x}As$ on top) structures(44). Both types of structures have sheet carrier concentrations of around 5 to 7 x $10^{11}cm^{-2}$. Normal HEMT structures have been fabricated into working transistors (Fig. 3), with a transconductance of 175 mS/mm at 77°K for 1.2 μm length gates. In Fig. 3, the gate biases are in 0.1 volt/step starting from zero volts.

The MBE used for our material growth is a Perkin-Elmer 425B system. It is a state-of-the-art, second generation, MBE system. It can accommodate a cassette of 6 wafers, up to 3 inches diameter, in its introduction chamber. The system is a conventional 3 chamber, ultra-high vacuum (UHV) vessel with base pressure ~5 x 10^{-11} Torr, and one chamber each used for sample introduction, analysis, and crystal growth. The 3 chambers are separated from each other by UHV valves.

The $GaAs/Al_xGa_{1-x}As$ epitaxial layers are grown from effusion cells containing elemental Al(6-9's purity), Ga(7-9's purity) and As(6-9's purity). The As_4 is reduced to the dimer As_2 species by passing it through a hot (≈1000°C) Mo tube. The n-type dopant used for our HEMT/inverted HEMT work is silicon, which has been float zone refined to lower its oxygen content.

The crystal growth is monitored by reflected high energy electron diffraction (RHEED) from which we can obtain real time information concerning the crystal morphology, surface roughness, and growth rate. Also in the growth chamber is a 0 to 400 AMU mass spectrometer which is used for monitoring background gasses and effusion cell fluxes.

Only inverted HEMT structures were grown for this program.

3.2 Materials Characterization

The standard method used to evaluate the inverted HEMT structures is the Hall Van-Der-Pauw Technique. From these measurements, one can obtain the two-dimensional electron concentration and the electron mobility at both room temperature and 77°K. We have also used low temperature (4.2°K) photoluminesence (PL) to evaluate the purity of our unintentionally doped GaAs layers. The spectra shows strong exciton emission. With PL, we have been able to spot acceptors, but are unable to

identify their type, i.e., whether they are copper or beryllium. There are very low concentrations of other acceptors at levels at least one order of magnitude lower.

A comment is in order here on the HEMT/inverted HEMT structure. Evaluation of the mobilities in this type of structure would be difficult because any Hall Van-Der-Pauw measurements will be measuring the mobilities of the two sheets of 2 DEGs electrons in parallel and giving an averaged result. One would, therefore, grow separate calibration structures of the regular HEMT and inverted HEMT immediately prior to growing the combined structure, under identical growth conditions. The electrical measurements on these calibration structures can then be related to the performance of the associated HEMT/inverted HEMT structure. Also, the top (inverted) structure can be chemically removed or etched off so that the lower (normal) structure can be measured.

IV DESIGN AND FABICATION OF OHMIC CONTACTS AND THE SLOW-WAVE CIRCUIT

4.1 Fabrication of Ohmic Contacts

The ohmic contacts to the electron population in the 2 DEG region was done by standard evaporation techniques. The alloy used was Ni/Au-Ge/Ag/Au. The samples were angle lapped at the ends to provide a greater contact area. Our metalizations were done by thermal evaporation in an ion pumped vacuum chamber with base pressure of 1×10^{-7} Torr. The chamber also has Ti sublimation pumping to reduce the partial pressures of reactive gasses during contact deposition. The contacts were then annealed at 450°C in an inert (N_2) atmosphere for one minute to alloy them. Resistivities as low as 0.7 ohm mm have been achieved in our FET devices by this method. An autocatalytic bath is then used to plate up the final gold contact to the desired thickness.

4.2 Design and Fabrication of Slow-Wave Circuit

As mentioned above, the slow-wave circuit required must be able to reduce the electromagnetic wave phase velocity by a ("slowness") factor of $\sim 10^3$ in order to efficiently couple to the drifting electrons. The circuit used was an interdigital electrode structure such as described by Swanenberg[45]. In this circuit, the electromagnetic waves that propagate along the interdigital electrodes couple with the drifting charge carriers. The electromagnetic wave phase velocity is, when the " finger" length is much longer than the "finger" width, given by[45]

$$V_\phi = \frac{f\lambda_o}{n}, \tag{4.1}$$

where λ_o is the period of the electrode structure (Figure 1), f is frequency, and n is an integer. Taking n = 1, $V\phi$ = carrier drift velocity = 3×10^7 cm/sec, one gets λ_o = 30 μm for f = 10 GHz and λ_o = 3 μm for f = 100 Ghz. Interdigital structures with the latter period are difficult to fabricate, although a "finger " width of 0.5 μm appears feasible[21].

For the subject investigation, finger widths of 1, 2, and 3 μm were prepared. A typical analysis is given below, following Swanenburg [45].

Consider a 2 μm finger width so that λ_o = 8 μm. Therefore, $K_o = 2\pi/\lambda_o = 7.85 \times 10^5$ cm^{-1}. We want $v_d > \omega/k_o = v_p$. Taking $v_d = 10^6$ cm/sec, a reasonable value, we obtain

$$f < \frac{v_d k_o}{2\pi} = 1.25 \times 10^{11}\, sec^{-1} \tag{4.2}$$

or 125 GHz. Taking f = 1 GHz, we obtain the value $v_p = 0.80 \times 10^4$ cm/sec. For amplification, we want $v_d > v_p$, which certainly is the case for f = 1 GHz.

Losses in a slow-wave circuit are proportional to the slowness factor[16]. They will be approximately 100 times as great for the solid-state plasma case as for the gas-plasma case, where the slowness factor is ~10.

Figure 4 shows a typical slow wave circuit magnified. Twenty interdigitating fingers were used.

4.3 Amplifier Fabrication

As mentioned earlier, only inverted HEMT structures were grown (see Figure 1). Ohmic contacts were placed at the ends of the material with the interdigital electrodes between (see Figure 5). Typically, the distance between ohmic contacts is 2.2 mm.

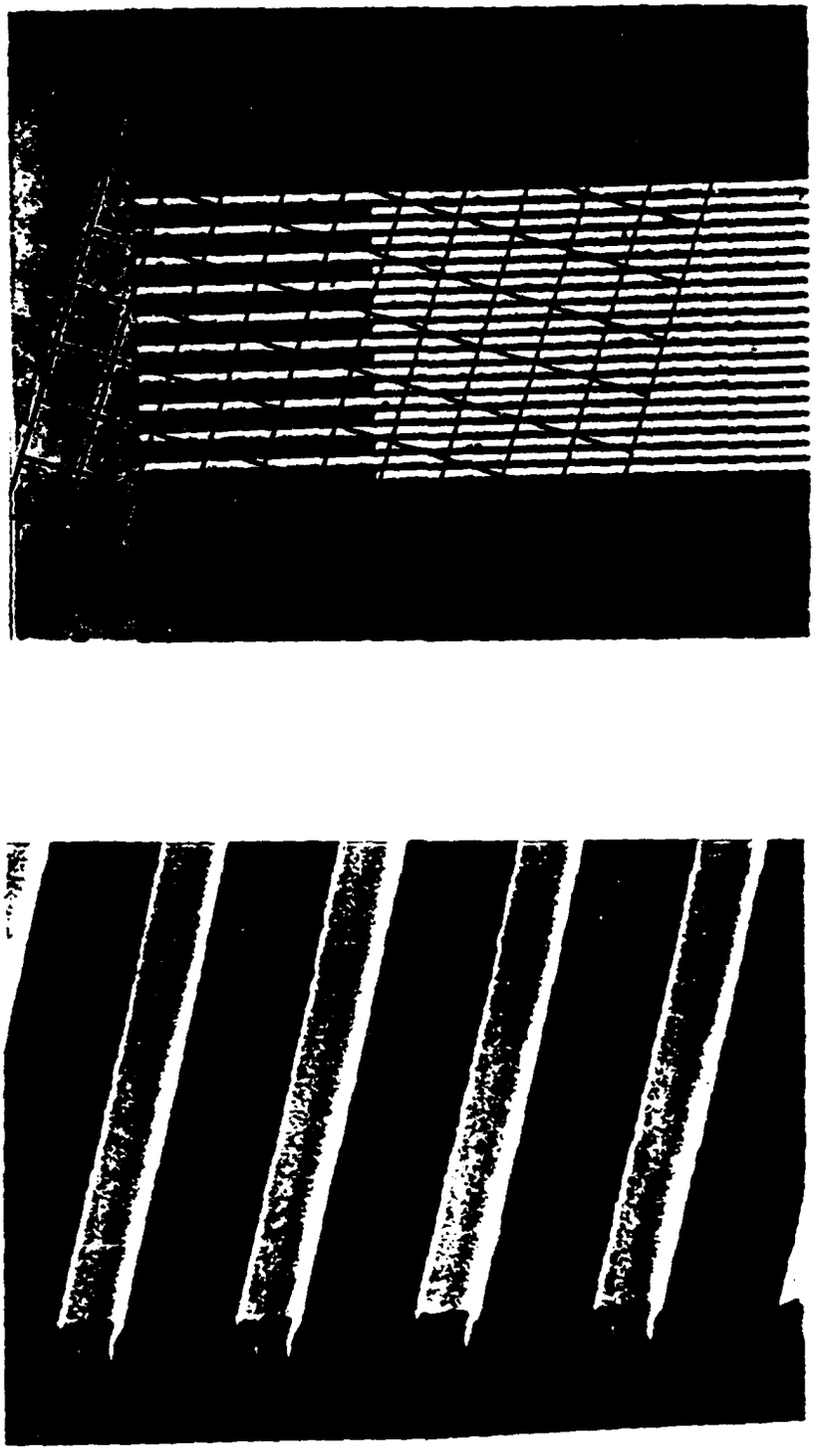

Figure 4. Interdigital Electrodes

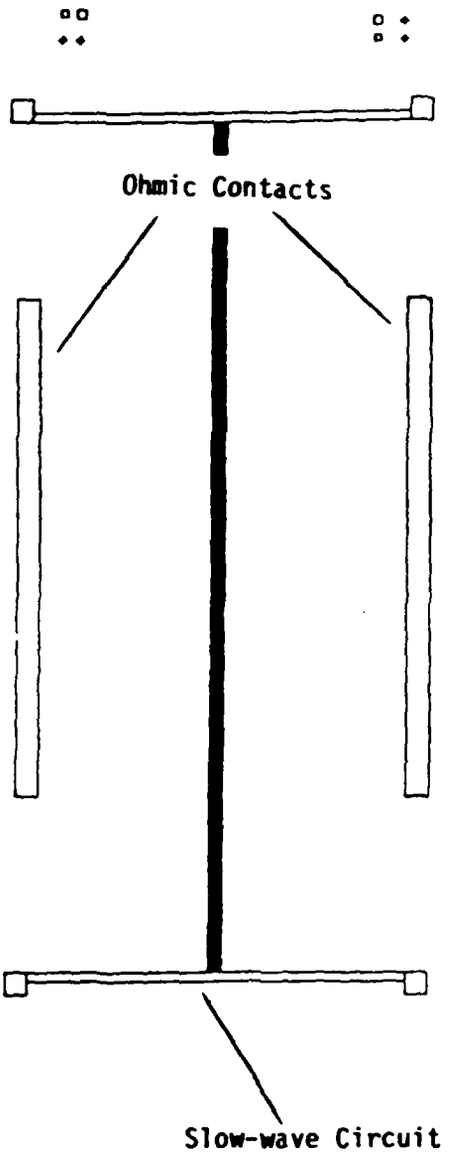

Figure 5. Slow-wave Circuit and Ohmic Contacts

V. AMPLIFIER TESTING

Of interest here was the interactive coupling between microwaves and the inverted HEMT channel electron stream. The slow-wave structure of the solid state device was designed to couple an external microwave signal into and out of the device. To investigate this, prototype devices (Figure 6) were utilized in a FET-like configuration with a dual gate and a source and a drain. Swept transmission and reflection measurements were made between a microwave input at Gate 1 and an output at the drain (Figure 7), using an automatic network analyzer (HP model 4508). The measurements were made in the frequency range 2.8 GHz - 7.6 GHz, which is within the expected frequency range of the slow-wave structure. It is compatible with the RF-DC hybrids utilized at the input and output. This measurement approach is essentially that described in Ref. 46.

Tests were made on two different devices. Device #1 has a slow-wave structure with 2 μm interdigital electrode finger widths, while device #2 has finger-widths of 3μm. Three biases were considered for gate 1, namely 0.1, -0.5, and -0.7 volt. For the drain biases, values in the range, 0.1 - 3 volts were utilized. Two temperatures were considered: ambient (300°K) and LN_2 (77°K).

Figure 8 shows, for the test setup of Figure 7, the percent of microwave transmission vs. drain bias for several gate biases. The transmission is relative to that for gate 1 and drain biases of zero. The input microwave frequency was 5.3 GHz.

Reversing the direction of microwave propagation in the slow-wave circuit so that it was in a direction opposite to that of the current flow significantly reduced the transmitted power.

These results (Figure 8) indicate that the microwave transmission increases both with increasing gate bias and with drain bias. This is interpreted to mean that there is coupling between the microwaves and the electron stream.

A second device (#2) was similarly tested and the results are shown in Figure 9. Here the test frequency was 4.5 GHz. The results are qualitatively the same as those of Figure 8.

Finally, Figure 10 shows the results of measurements made at 77°K. These results differ from those taken at room temperature in that microwave transmissivity doesn't substantially increase with either gate or drain bias. For $V_D > 2$ volts, however, there is some indication that the microwave transmissivity is increasing slightly with gate and drain bias. The microwave attenuation at 77°K was reduced by 2 - 3 dB compared with that of 300°K

From these experimental results, it is concluded that there is coupling of microwaves - through the slow wave circuit - and drifting electrons, certainly at 300°K. The results at 77°K, however, are different from those at 300°K and are not understood at this time.

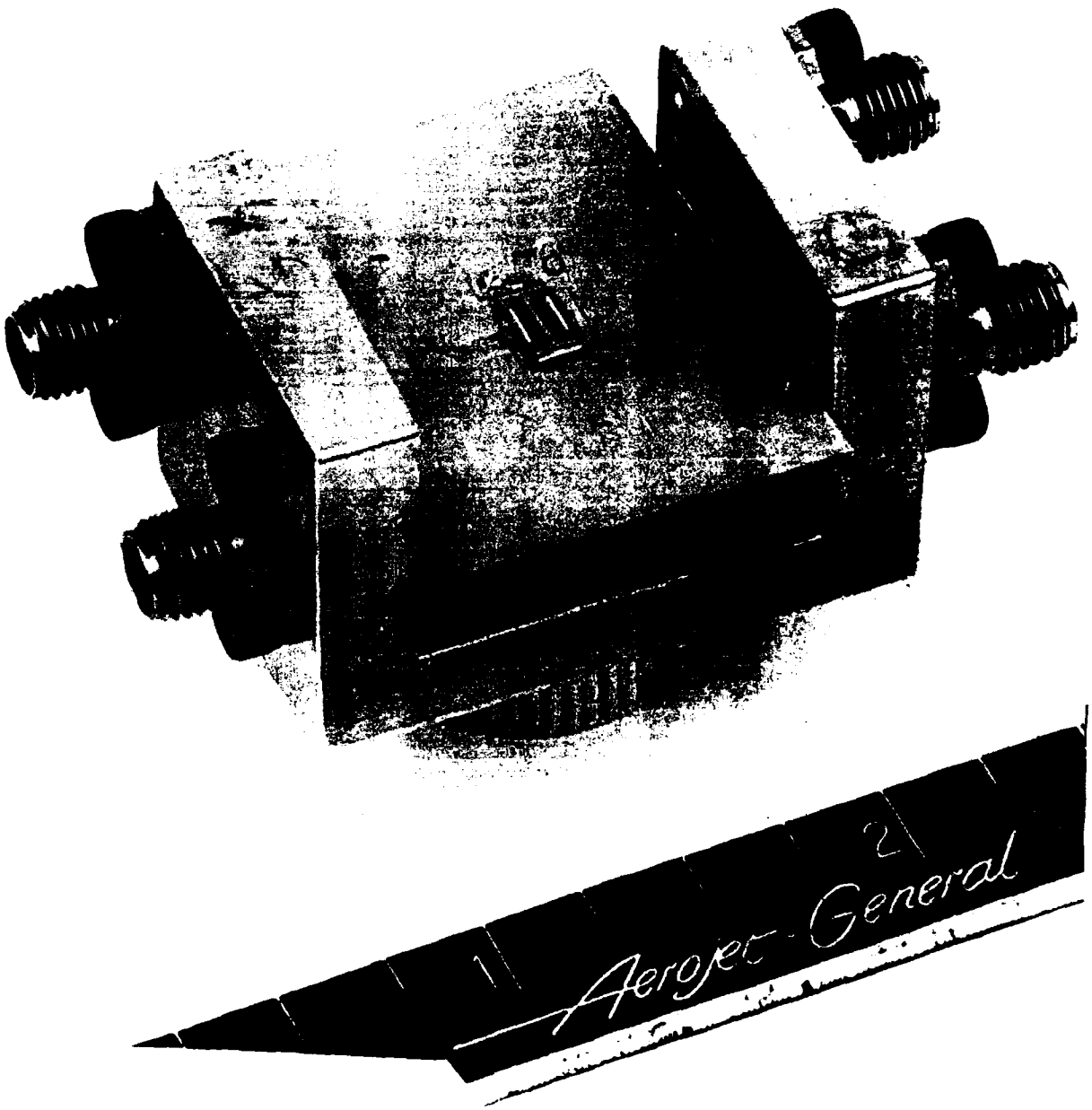

Figure 6. Prototype Space-charge-wave Solid State Microwave Amplifier

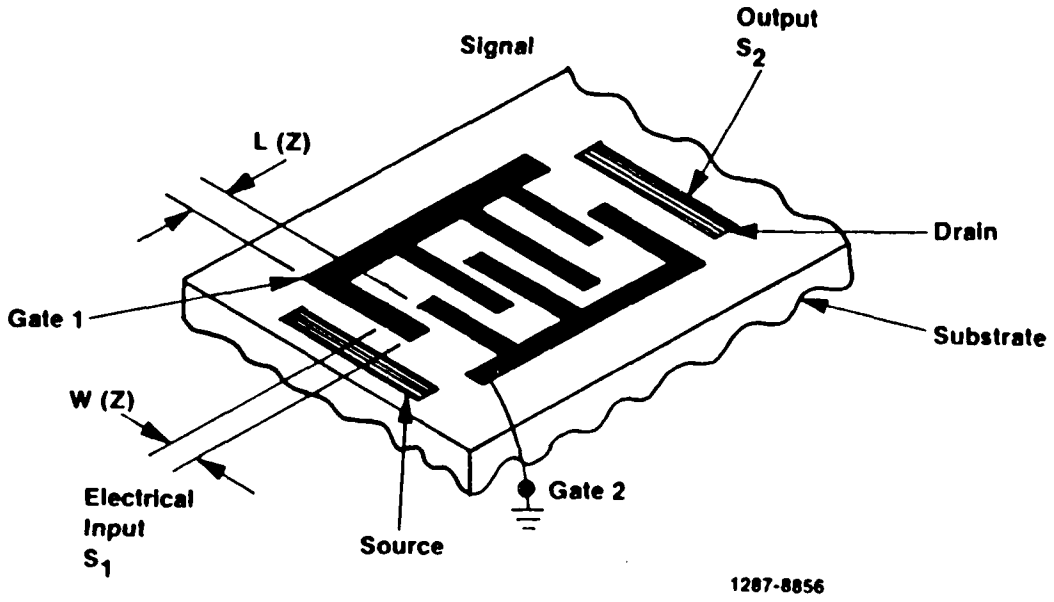

Figure 7. Experimental Setup

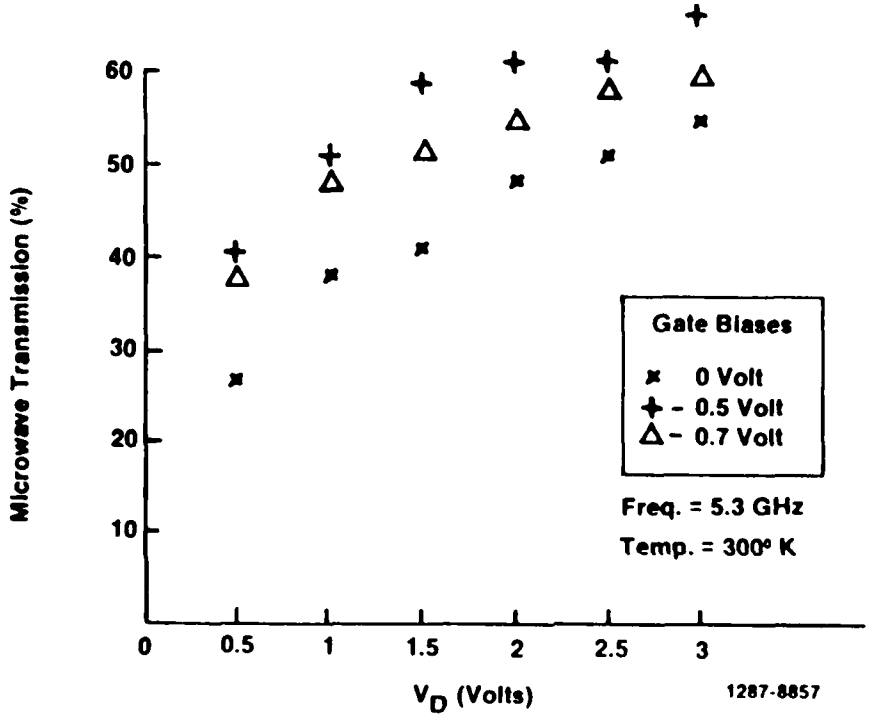

Figure 8. Microwave Transmission vs. Drain Bias for Several Gate Biases-device #1.

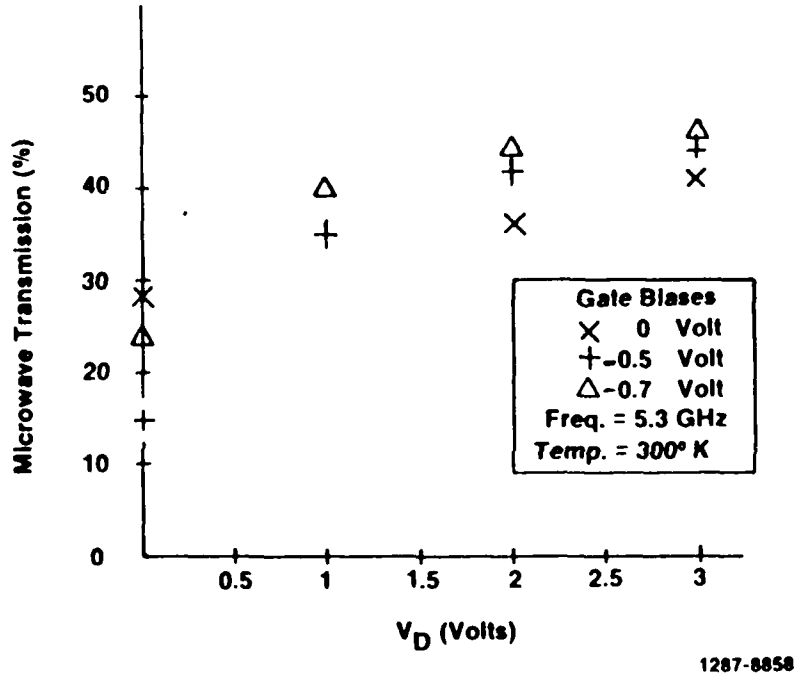

Figure 9. Microwave Transmission vs. Drain Bias for Several Gate Biases-device #2.

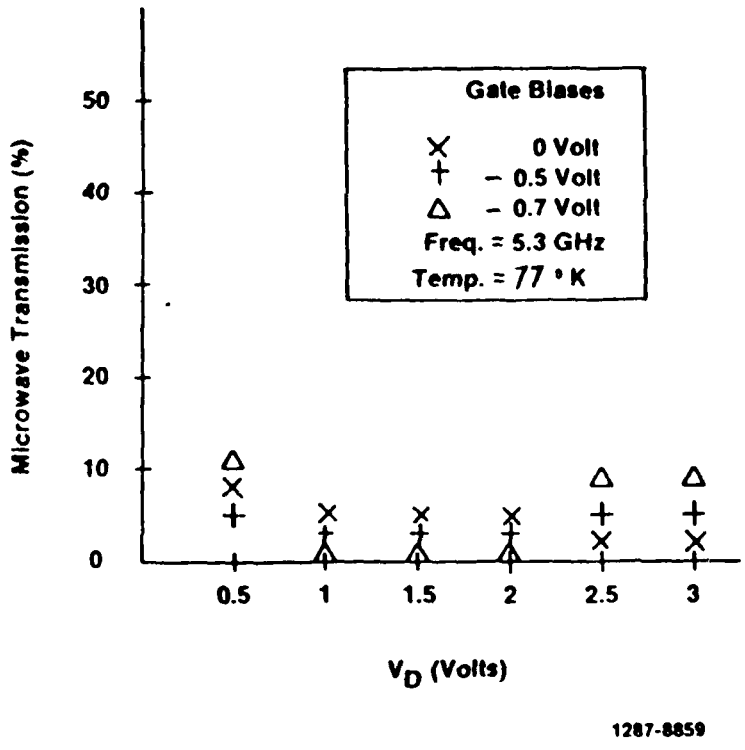

Figure 10. Microwave Transmission vs. Drain Bias for Several Gate Biases-device #1 at 77°K.

VI. THEORY

In what follows, results are given from two theoretical investigations: (1) Theory of Optical Phonon-Space Charge Wave Interactions in Doped GaAs, and (2) Theory of the Interaction of Electromagnetic Waves and Drifting Electrons in Modulation-Doped AlGaAs/GaAs Heterostructures. Preliminary results for item (1) were presented at an APS meeting[47].

6.1 Theory of Optical Phonon-Space Charge Wave Interactions in Doped GaAs

A theoretical investigation has been made of the interaction of optical phonons and space charge waves in a solid state plasma, namely doped GaAs. In obtaining the dispersion relation, the specular-reflection approach of Kliewer and Fuchs was used. Dispersion curves have been obtained taking into account carrier damping. Results indicate that space charge wave amplification occurs for certain frequency ranges.

6.1.1 Introduction

Surface electromagnetic wave instabilities in doped semiconductors (solid state plasmas) have been the subject of many theoretical and experimental investigations[48] over the past three decades. Of particular interest is the possibility of amplifying surface waves by drifting current carriers. The subject of this paper was considered previously by Tajima and Ushioda[49], but they did not take into account carrier damping. In addition, their dispersion relation did not account correctly for the spatial dispersion.

In what follows, we obtain the electromagnetic wave dispersion relation for polar semiconductors using the specular-reflection boundary conditions of Fliewer and Fuchs[30] (Section 6.1.2). Calculated results are then presented for doped GaAs in Section 6.1.3, taking into account carrier damping. In addition, the results of an analysis of dispersion instabilities are given. Finally, in Section 6.1.4, conclusions are presented.

6.1.2 Theory

Consider a semiconductor which is infinite in the x- and y- directions and semi- infinite in the z- direction (Figure 11). The other half-space is filled by a dielectric. In what follows, we will use the nonlocal Maxwell equations for this geometry to obtain expressions relating the field and dielectric tensor components. The specular-relection technique of Fliewer and Fuchs will be used to obtain the dispersion relation.

In seeking solutions to the Maxwell equations, it is assumed that the Cartesian components of the electric field E have the form

$$\bar{E}(\bar{r},t) = [O, \bar{E}_y(z), \bar{E}_z(z)] \exp[i(k_y y - \omega t)] ,$$

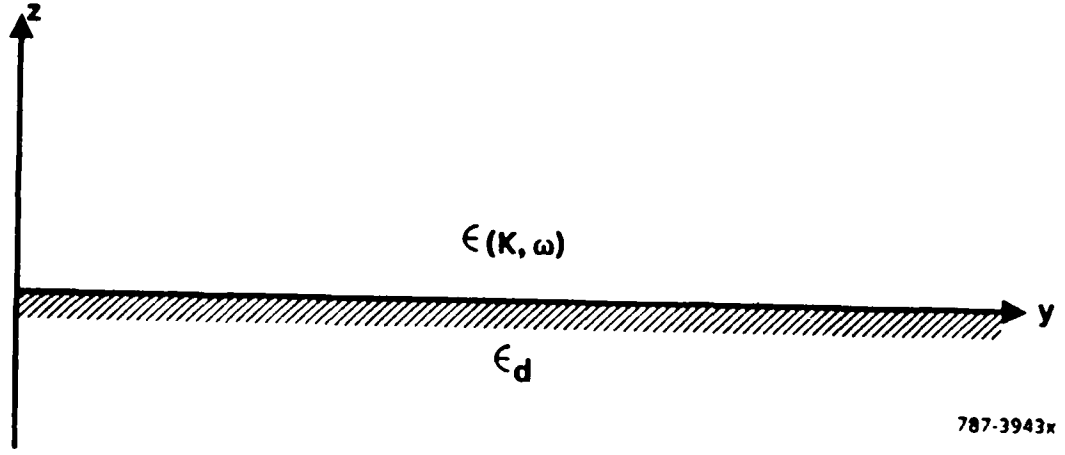

Figure 11. Problem Geometry

Where k_y is the wave vector and ω is the frequency. Similar forms are used for the displacement D and the magnetic field B. Only p-polarization will be considered, i.e., the situation where the electric vector lies in the sagittal plane defined by the direction of propagation and the normal to the surface.

Following the Kliewer-Fuchs specular-reflection approach, the surface polariton dispersion relation is given by

$$1 + \frac{\omega^2 \varepsilon_d}{\pi c^2 a_o} \int_{-\infty}^{\infty} dk_z \, \frac{T_{zz}}{T_{zz} T_{yy} - T_{yz}^2} = 0 \, , \tag{6.1}$$

where a_o is the decay coefficient for the vacuum and is given by

$$a_o^2 = k_y^2 - \frac{\omega^2}{c^2} \, , \tag{6.2}$$

and the quantities in the integrand of Eq. (6.1) are given by

$$T_{yy} = \frac{\omega^2}{c^2} \varepsilon_{yy}(\bar{k}, \omega) - k_z^2 \, , \tag{6.3}$$

$$T_{zz} = \frac{\omega^2}{c^2} \varepsilon_{zz}(\bar{k}, \omega) - k_y^2 \, , \tag{6.4}$$

and

$$T_{yz} = T_{zy} = \frac{\omega^2}{c^2} \varepsilon_{yz}(\bar{k}, \omega) + k_y k_z \tag{6.5}$$

To obtain $\varepsilon_{\alpha\beta}$, we proceed by linearizing the transport equation for the motion of an average carrier in the semiconductor. The nonlocal conductivity tensor thus obtained is

$$\sigma_{\alpha\beta}(\bar{k}, \omega) = N_o q \left[\overline{M}_{\alpha\beta}(\bar{k}, \omega) + \frac{V_{\infty}}{\omega - \bar{k} \cdot \bar{V}_o} \sum_{\gamma} k_{\gamma} \overline{M}_{\gamma\beta}(\bar{k}, \omega) \right] \, , \tag{6.6}$$

Where N_0 is the equilibrium carrier density, V_0 is the drift velocity, and the matrix M is given by

$$\overline{M}_{\alpha\beta} = \frac{iq}{a} \begin{pmatrix} \omega-(k_y V_{oy}+k_z V_{oz}) & k_x V_{oy} & k_x V_{oz} \\ k_y - V_{ox} & \omega-(k_x V_{oy}+k_x V_{oz}) & k_y V_{oz} \\ k_z V_{ox} & k_z V_{oy} & \omega-(k_x V_{ox}+k_y V_{oy}) \end{pmatrix} \tag{6.7}$$

with $a = m^* \omega (\omega - k \cdot V_0 + i\nu)$, where m^* is the carrier effective mass and ν is the carrier damping. The components of the dielectric tensor are given by

$$\varepsilon_{\alpha\beta}(\bar{k},\omega) = \delta_{\alpha\beta}\varepsilon_\infty + \frac{4\pi i}{\omega}\sigma_{\alpha\beta} , \tag{6.8}$$

where $\delta_{\alpha\beta}$ is the Kronecker delta and ε_∞ is the background dielectric constant.

We have already obtained the dielectric tensor for the case of a dc current interactive with surface polaritons in a nonpolar semiconductor[50]. We now consider the case of a polar semiconductor, where the interaction of surface space charge waves and surface optical phonons must be taken into account. This is quite easy as far as components of the dielectric tensor are concerned. One merely needs to add the form

$$\varepsilon_\infty \left(\frac{\omega_L^2 - \omega_T^2}{\omega_T^2 - \omega^2} \right)$$

to the diagonal elements of the dielectric tensor. In this expression ω_L is the longitudinal optical phonon frequency and ω_T is the transverse optical phonon frequency.

For the geometry of interest here, namely $k = (o,k_y,k_z)$ and $V_0 = (o,V_{oy},o)$ the dielectric tensor is given by Eq. (6.8) with ε_∞ replaced by ε_p, where

$$\varepsilon_p = \varepsilon_\infty \left(1 + \frac{\omega_L^2 - \omega_T^2}{\omega_T^2 - \omega^2} \right) . \tag{6.9}$$

The tensor components are

$$\varepsilon_{yy} = \varepsilon_p \left[1 - \frac{\omega_p^2}{\omega^2} \frac{\left(\omega^2 + k_z^2 V_{oy}^2\right)}{(\omega - k_y V_{oy} + i\nu)(\omega - k_y V_{oy})} \right] , \tag{6.10}$$

Where ω_p^2 is an effective plasma frequency

$$\omega_p^2 = 4\pi N_o q^2/\varepsilon_p m^* \quad , \tag{6.11}$$

Note that $\varepsilon_p\omega_p^2 = \varepsilon_\infty\omega_e^2$

$$\varepsilon_{zy} = \varepsilon_{yz} = -\varepsilon_p \frac{\omega_p^2}{\omega^2} \frac{k_z V_{oy}}{(\omega - k_y V_{oy} + i\nu)} \quad , \tag{6.12}$$

$$\varepsilon_{zz} = \varepsilon_p \left[1 - \frac{\omega_p^2}{\omega^2} \frac{(\omega - k_y V_{oy})}{(\omega - k_y V_{oy} + i\nu)}\right] \quad . \tag{6.13}$$

Using these tensor elements, one obtains the dispersion relation from Eq. (6.1); namely

$$\frac{\varepsilon_p}{\varepsilon_d}\left[1 - \frac{\omega_p^2}{(\omega - k_y V_{oy})(\omega - k_y V_{oy} + i\nu)}\right]\left[1 - \frac{\varepsilon_p \omega_p^2 \frac{V_{oy}^2}{c^2}}{\omega_p^2 - (\omega - k_y V_{oy})(\omega - k_y V_{oy} + i\nu)}\right]^{1/2} = -\frac{a}{a_o} \quad , \tag{6.14}$$

where

$$a^2 = k_y^2 - \frac{\varepsilon_p}{c^2}\left[\omega^2 - \omega_p^2 \frac{(\omega - k_y V_{oy})}{(\omega - k_y V_{oy} + i\nu)}\right] \quad . \tag{6.15}$$

It is of interest to consider the dispersion relation for the non-retarded limit (i.e., $c \to \infty$):

$$\frac{\varepsilon_p}{\varepsilon_d}\left[1 - \frac{\omega_p^2}{(\omega - k_y V_{oy})(\omega - k_y V_{oy} + i\nu)}\right] = -1. \tag{6.16}$$

Neglecting damping, one obtains the result

$$k_y = \frac{\omega}{V_{oy}} \pm \frac{\omega_e}{V_{oy}}\left[\frac{\varepsilon_\infty(\omega_T^2 - \omega^2}{\omega_T^2 + \varepsilon_\infty\omega_L^2 - \omega^2(1 + \varepsilon_\infty)}\right]^{1/2} \quad , \tag{6.17}$$

Where ε_d has been taken to equal 1 (vacuum layer). For frequencies in the range

$$\omega_T^2 < \omega^2 < \frac{\omega_T^2 + \varepsilon_\infty \omega_L^2}{1 + \varepsilon_\infty}, \tag{6.18}$$

the expression under the radical in Eq. (6.17) is negative and hence k_y consists of complex-conjugate pairs. For the (+) sign we have an exponentially decaying wave, while for the (-) sign, we have an exponentially amplified wave. Note from Eq. (6.17) that the slow SCW gain increases with increasing plasma frequency, ω_e, i.e., with increasing carrier concentration. When the frequency ω lies outside the range given by Eq. (6.18), there are no amplifying or decaying waves. Note that, in the absence of optical phonons, Eq. (6.17) reduces to

$$k_y = \frac{\omega}{V_{oy}} \pm \frac{\omega_e}{V_{oy}} \left(\frac{\varepsilon_\infty}{1 + \varepsilon_\infty} \right)^{1/2}, \tag{6.19}$$

the dispersion relation for space charge waves. Here the wave vector is real; hence, it is the presence of optical phonons that give rise to amplifying instabilities.

6.1.3 Results and Discussion

Theoretical dispersion curves have been obtained for surface waves in GaAs in the presence of drifting current carriers. The effects of retardation and spatial dispersion are included, as is the effect of damping resulting from the scattering of carriers. Optical phonon damping is neglected because it is generally small compared with carrier damping. In the calculations, the frequency ω was taken as real and the dispersion relation was solved for wave vector k_y.

For GaAs, at 300°K, $\varepsilon_o = 12.85$ and $\varepsilon_\infty = 10.88$[51]. The Lyddane-Sachs - Teller relation is

$$\frac{\varepsilon_o}{\varepsilon_\infty} = \frac{\omega_L^2}{\omega_T^2}, \tag{6.20}$$

which gives the result

$$\frac{\omega_L}{\omega_T} = 1.18. \tag{6.21}$$

Non-retarded Limit

For the non-retarded limit, the dispersion relation, neglecting carrier damping, is given by Eq. (6.17). This equation was used to obtain the dispersion results shown in Figure 12.

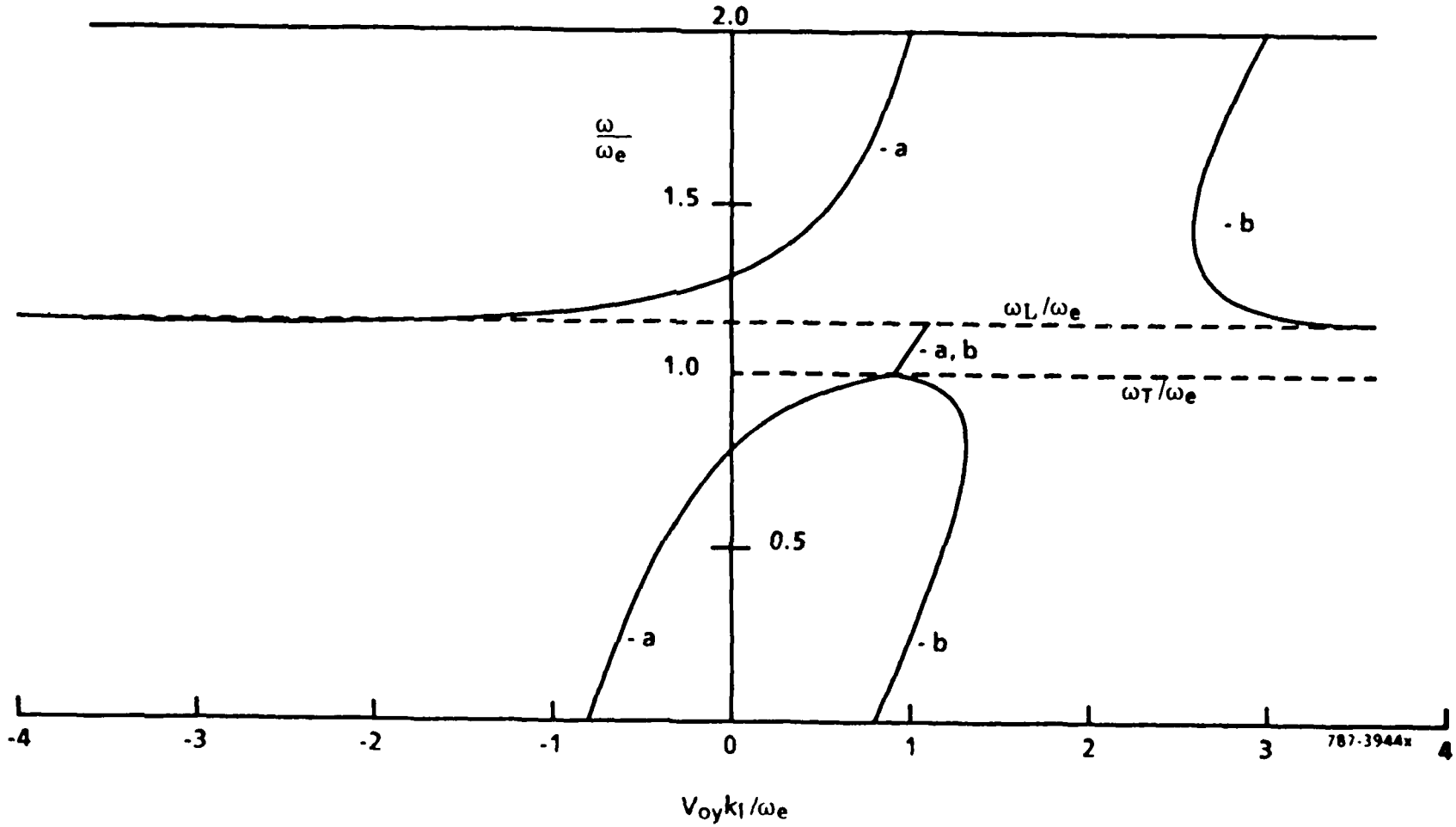

Figure 12. Dispersion Curves in the Nonretarded Limit

For frequencies $\omega < \omega_e$ there are two space charge wave (SCW) branches labeled a and b, where a is the fast SCW branch and b is the low SCW branch. At $\omega = \omega_T$, the two branches merge, (branch c), with the result that there are complex-conjugate wave vectors, one of the pair corresponding to an amplifying SCW/optical phonon instability. Near $\omega = \omega_L$ (See Eq. (6.18), branch c splits and we recover the two SCW branches a and b.

The frequency dependence of the imaginary part of the wave vector for branch c is shown in Figure 13. The gain (and decay) increases with increasing frequency from $\omega > \omega_T$, where it starts, then abruptly drops to zero just below $\omega > \omega_L$. The gain becomes infinite only because damping has been neglected.

Retardation Effect Neglecting Carrier Damping

Next we consider the dispersion relation including retardation, namely Eq. (6.14). This equation is of 4th degree in wave vector and so two more branches result in the dispersion relation. Figure 14a shows the dispersion for positive values of wave vector, while Figure 14b shows that for negative values of wave vector. Note that the normalization of wave vector has been changed to ck_y/ω_e from $V_{oy}\, k_y/\omega_e$.

First consider the dispersion neglecting carrier damping. For frequencies $\omega < \omega_T$, we have, in Figures 14a and 14b, the SCW branches SCW+ and SCW-, but displaced. In addition, we have the plasmon branches P+ and P-. At small values of wave vector, branch P+ (Fig. 14a) is plasmon-like, but then becomes SCW-like for frequencies $\omega > 0.8\ \omega_e$. At $\omega = \omega_T$, branches P+ and SCW+ interact with the optical phonon-mode, producing complex-conjugate wave vectors. Here the slow SCW (branch SCW+) and the optical phonons interact producing amplification of the slow SCW, while the fast SCW-phonon interaction is evanescent. In effect, the fast SCW is losing energy to the slow SCW via the optical phonons.

Turning to Figure 14b, we see that branch P-, the plasmon-mode, couples with branch SCW-, the fast SCW-mode, the resulting curve representing an evanescent interaction. This behavior also occurs in the absence of phonons[50].

Returning to Figure 4a, note that at $\omega < \omega_L$, the degenerate branch P+, SCW+ splits, branch P+ moving toward-negative infinite and branch SCW+ moving toward positive infinity. At frequencies slightly higher than $\omega = \omega_L$, the branches move rapidly toward smaller wave vector values, with branch SCW+ bending upward (Fig. 14a).

At $\omega = \omega_T$, in Figure 14a, the usual optical phonon dispersion (branch P+) begins, but with increasing frequency is not asymptotic to ω_L, as is the usual situation in the absence of plasmons and SCWs. Instead, it bends to the right and then moves upward, becoming essentially parallel to branch SCW+.

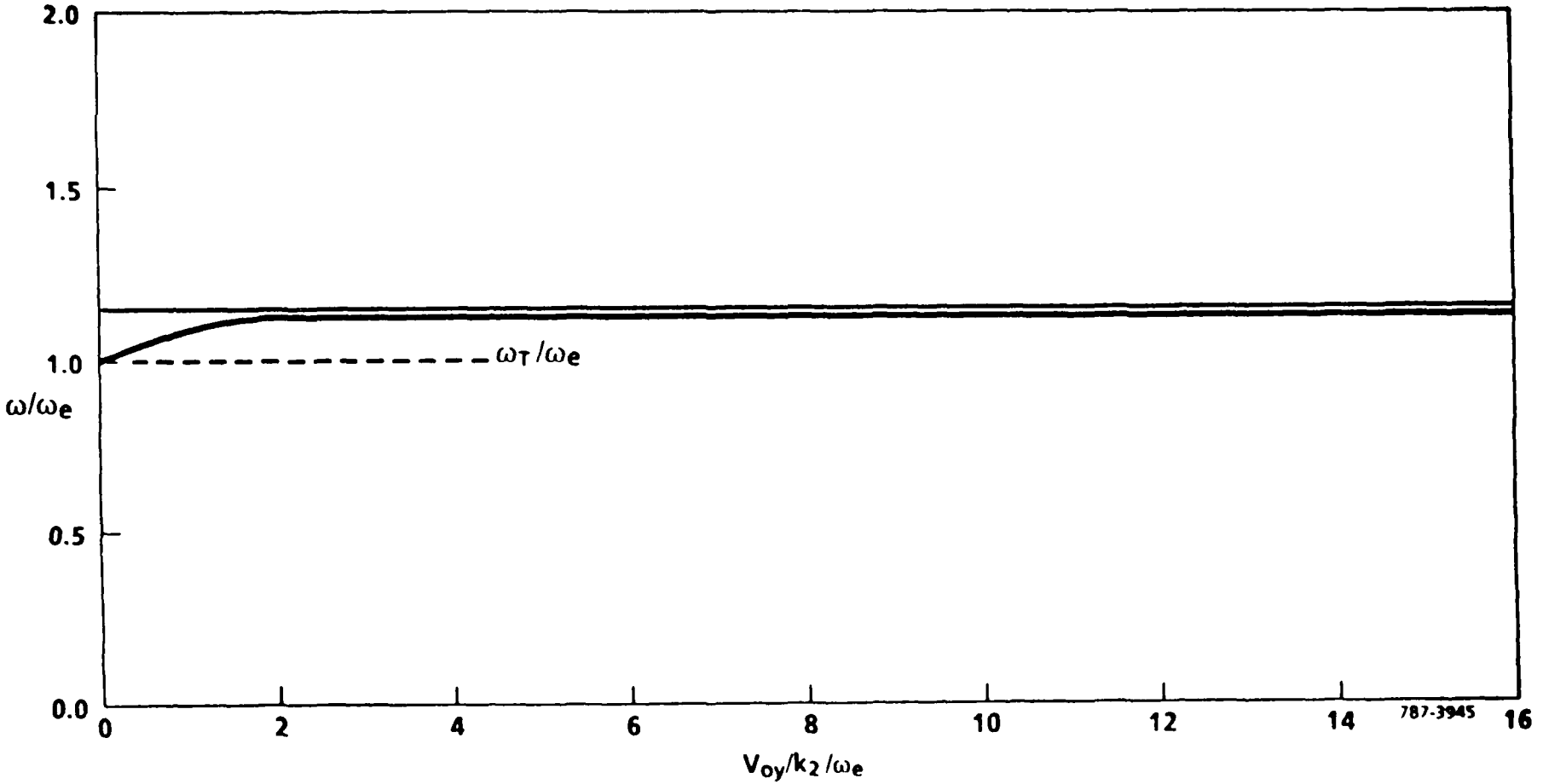

Figure 13. Frequency Dependence of the Imaginary Part of the Wave Vector in the Nonretarded Limit.

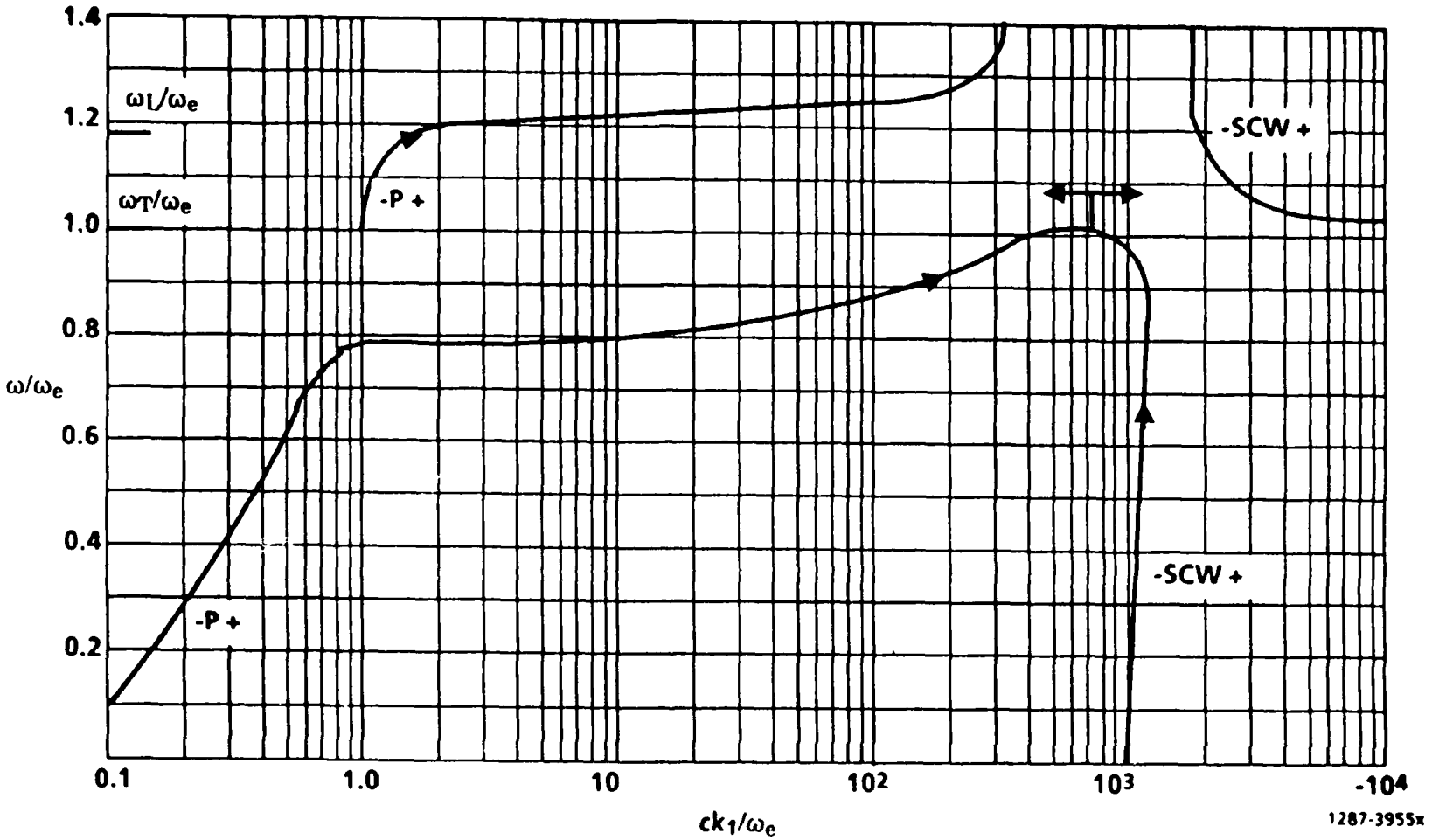

Figure 14. Dispersion Curves with Retardation

(a) Positive wave vectors

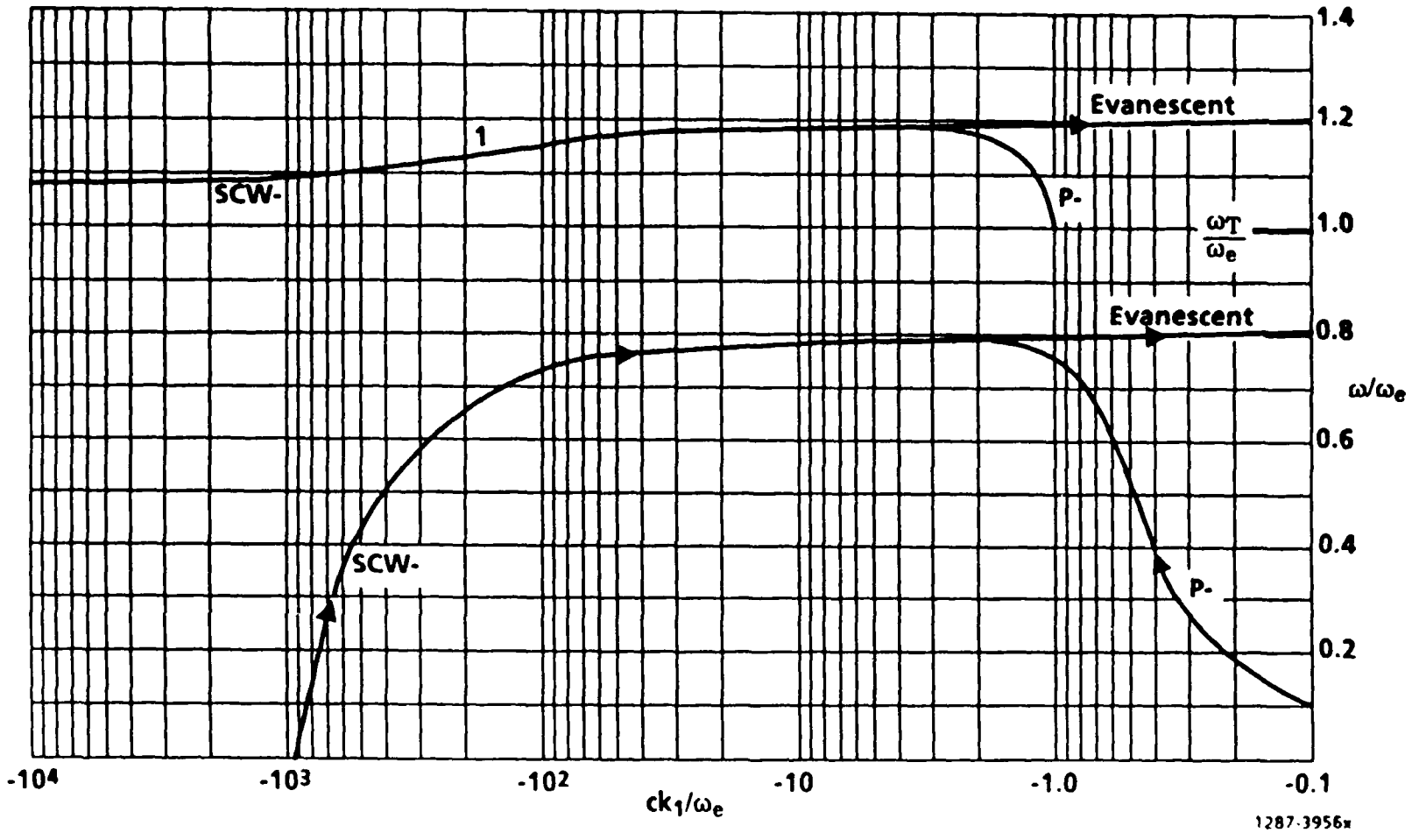

(b) Negative wave vectors

At $\omega = \omega_T$, in Figure 14b, we also have an optical phonon branch beginning (branch P-) and this shows behavior similar to that of branch P+, except that it intercepts the SCW branch, forming a branch composed of complex-conjugate wave vectors, which is evanescent. Figure 15 shows the frequency-dependence of the imaginary part of the wave vector for the amplifying mode.

Retardation Effects With Carrier Damping

Figures 16a and 16b show the dispersion curves for the situation where damping is included. The presence of damping makes noticeable changes. Consider Figure 16a. In contrast to Figure 14a, branch P+ does not bend over to interact with branch SCW+ in Figure 16a; instead, it is branch SCW- (the fast SCW) that interacts with branch SCW+ (the slow SCW) giving rise to amplification of the slow SCW. This degenerate branch splits for frequencies $\omega \sim \omega_L$, similar to what we have seen in Figure 14a. Note that the behavior of the slow SCW, branch SCW+, is essentially the same in both Figures 14a and 16a.

The behavior shown in Figure 16b is also different than that of Figure 14b. The plasmon branch P- does not interact with the fast SCW branch (SCW-). They cross, but there is no indication of an interaction. Thus, one concludes that the presence of damping eliminates evanescent interactions shown in Figure 14b, but does not prevent amplification of the slow SCW branch.

Plasma instabilities require analysis to determine whether or not they are amplifying. *One such analysis is that of Sturrock*[31], *another was provided by* Sudan[52]. The latter approach was used here because the dispersion relation (Eq. 6.17) is relatively simple. A Sudan analysis goes as follows:

Consider the dispersion relation $D(k, \omega) = 0$. Obtain the n roots, $k_n(\omega)$, and then take $\omega = \omega_1 + \omega_2$. The instability characterization proceeds as follows for each $k_n(\omega)$:

1. Casualty requirement

$$\lim_{\omega_2 \to \infty} R_e\,(ik) \to -\infty$$

2. Convective instability

$$R_e\,(ik) > 0 \quad \text{for } \omega_2 = 0$$

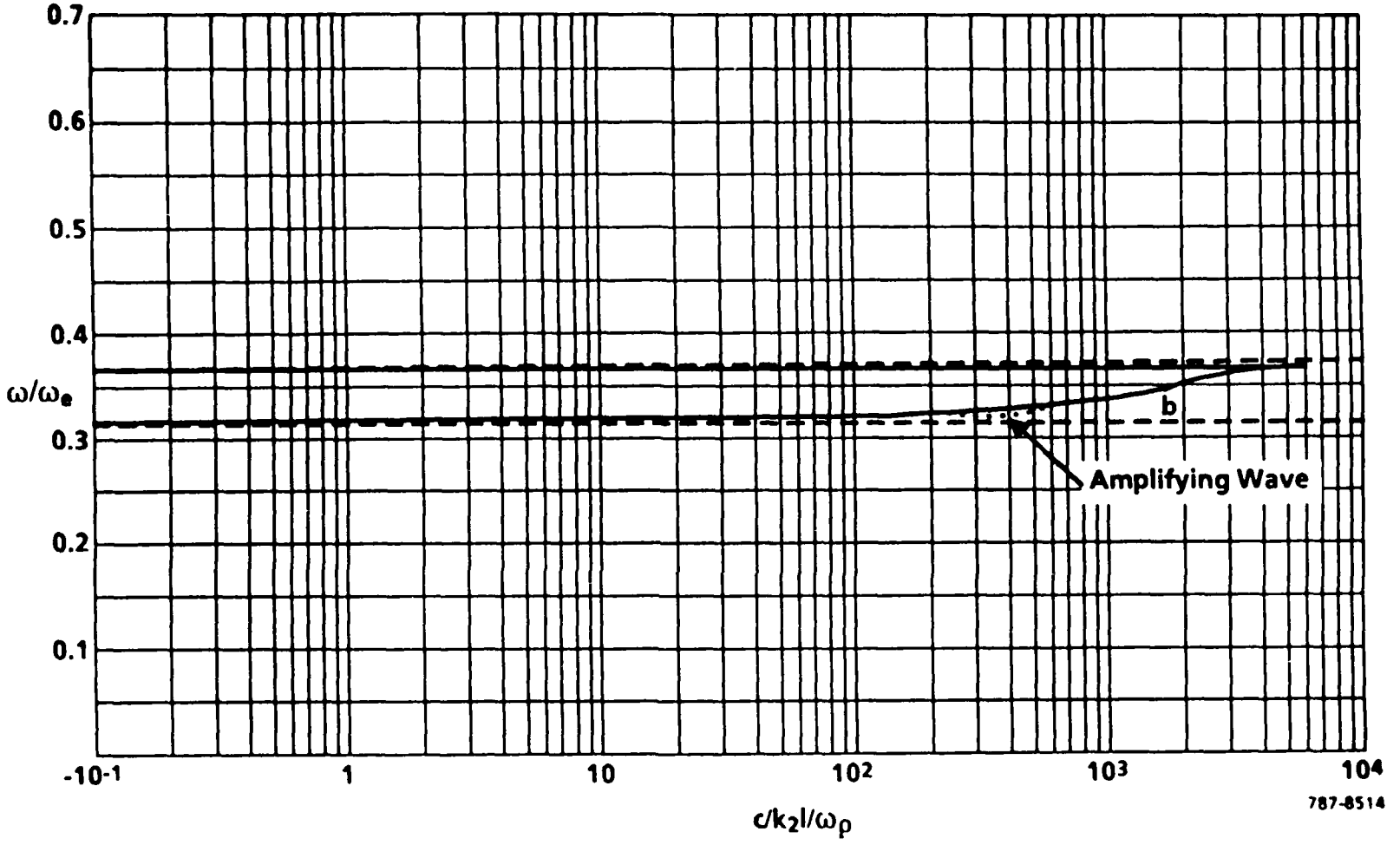

Figure 15. Frequency Dependence of the Imaginary part of the Wave Vector with Retardation.

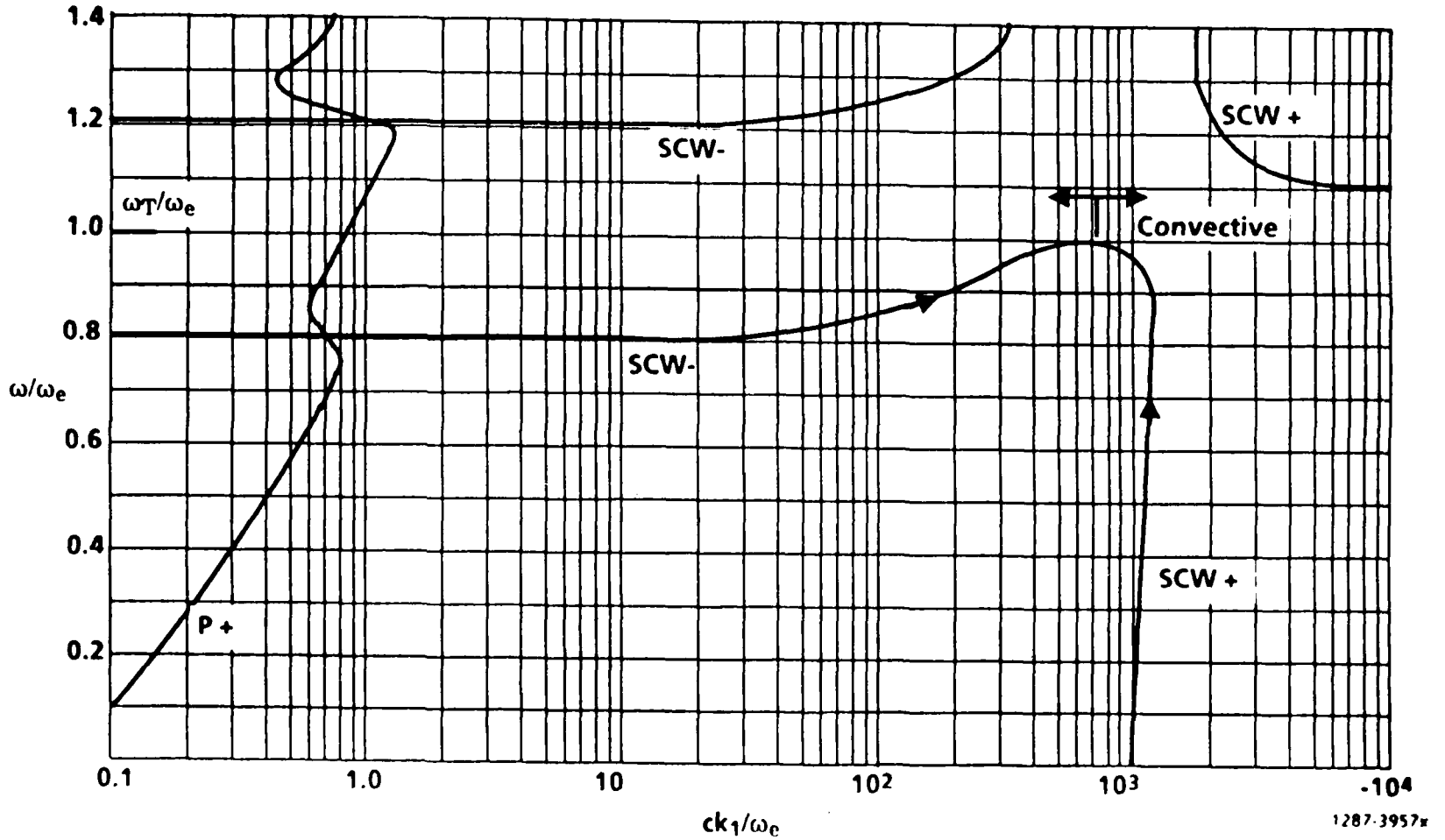

Figure 16. Dispersion Curves with Retardation and Damping
(a) Positive wave vectors

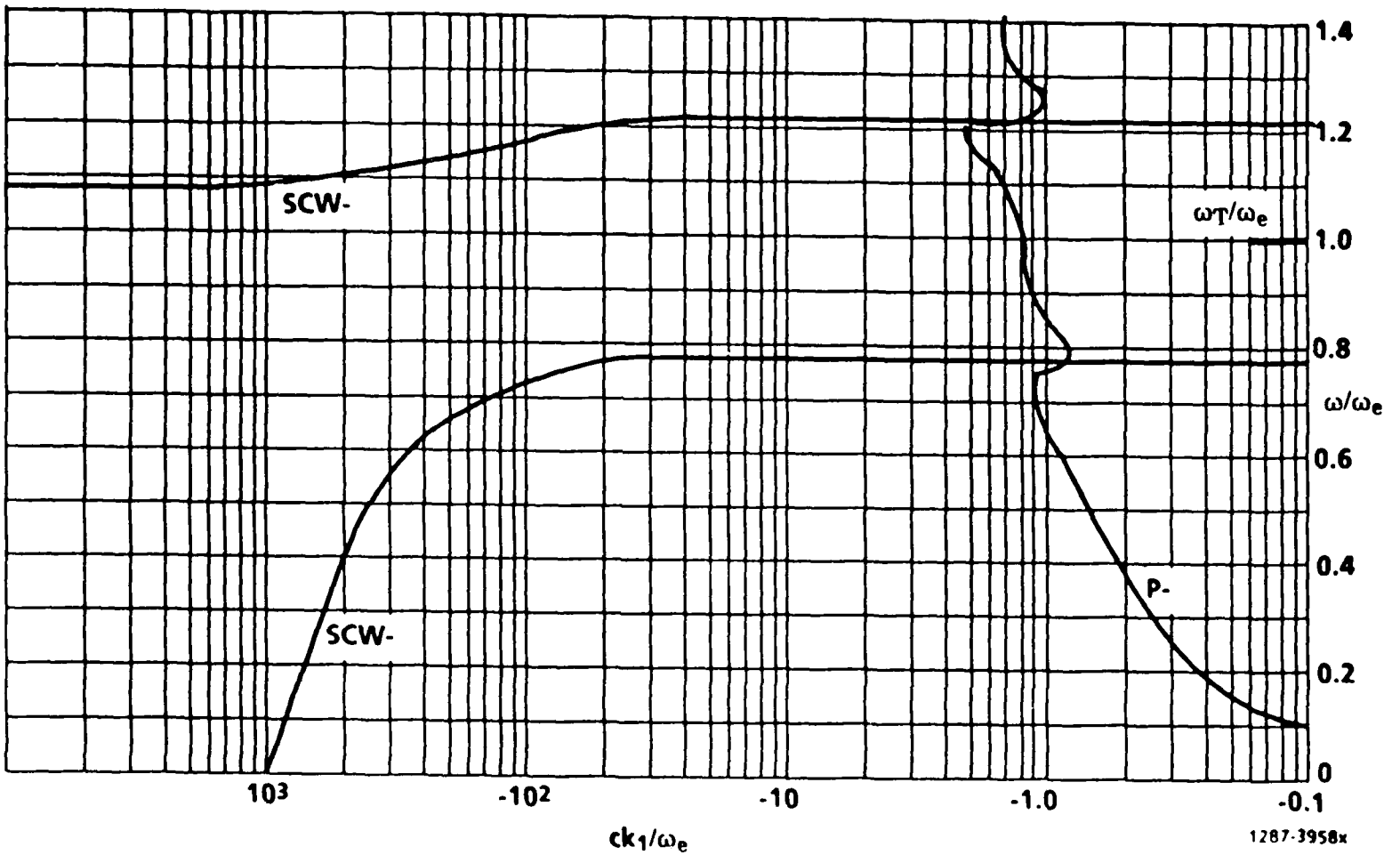

(b) Negative wave vectors

3. Absolute or nonconvective instability

$$\frac{dk}{d\omega} \rightarrow \infty \text{ for } \omega_2 > 0$$

Performing this analysis on Eq. (6.17) shows that the slow SCW associated with degenerate branches are amplifying, as stated above. What is interesting from the above results is that the TO phonons act, in effect, like the resistive wall of Birdsall et al, (10), namely giving slow-SCW amplification.

It was mentioned previously that Tajima and Ushioda(49) had considered this problem. They obtained dispersion relations both taking into account and neglecting a drift current. To obtain the former, they changed the latter by merely replacing ω_e^2/ω^2 by $\omega_e^2/(\omega - kv_D)^2$, where ω_e is the plasma frequency and v_D is the drift velocity. As can be seen from our formulation, this replacement neglects some of the tensor elements of $\varepsilon_{\alpha\beta}$, which are nonzero when a drift current is taken into account. Consequently, the dispersion relation of Tajima and Ushioda is incomplete.

It is of interest here to comment on mechanisms that would limit the carrier drift velocity. This is of interest because it bears on the coupling of electromagnetic waves and a drift current: for coupling to occur, $V_{oy} \simeq v_p$. For doped GaAs, the carrier mobility - and hence drift velocity - would be limited primarily by ionized impurity scattering. If the carriers are shunted away from ionized impurities, as they are in a GaAs/AlGaAs HEMT structure, then the factors limiting drift velocity are the creation of LO-optical phonons and Landau damping. The former loss mechanism was discussed previously. Landau damping is collisionless, and is non-linear and non-local with respect to the electric field. The loss mechanism is this(9): carriers whose drift velocity is slightly less than the phase velocity of the electromagnetic absorb energy from the wave, thus attenuating it. However, carriers whose drift velocity is slightly greater than the phase velocity will amplify the electromagnetic wave. Landau damping has not been considered here, but would be of interest as future work.

6.2 Theory of the Interaction of Electromagnetic Waves and Drifting Electrons in Modulation-Doped AqGaAs/GaAs Heterostructures

6.2.1 Introduction

A preliminary theoretical investigation has been made of the interaction of electromagnetic waves and drifting electrons in an AlGaAs/GaAs modulation-doped heterostructure. This structure was modeled as a three-layer medium (the middle layer being the electron channel); and the dispersion relation, including retardation, was obtained using the specular-reflection boundary conditions of Kliewer and Fuchs(30). Of particular interest are those interactions giving rise to amplifying instabilities.

6.2.2 Theory

The modeling geometry is shown in Figure 17. One medium occupies the space $Z \geq 0$, another the space $Z \leq -d$. These two media are separated by a third, $0 > Z > -d$. the dc electric field direction is taken to be in the y-direction, as is the direction of propagation of the electromagnetic waves.

The elements of the dielectric tensor for a semiconductor containing free carriers drifting in a static electric field can be derived from the transport equation for the motion of an average carrier, namely

$$\dot{\bar{V}} + (\bar{V}\cdot\bar{\nabla})\bar{V} = -\frac{\nabla P}{m^* N} + \frac{q}{m^*}\left(\bar{E} + \frac{1}{c}\,\bar{V} \times \bar{H}\right) - \nu\,\bar{V}, \tag{6.22}$$

and the continuity equation

$$\dot{N} + \bar{\nabla}\cdot(N\bar{V}) = 0, \tag{6.23}$$

where V, ν, m^*, q, and N are, respectively, the carrier velocity, collision frequency, effective mass, charge and particle density, ∇P is the carrier thermal pressure gradient, and E and H are the total electric and magnetic field, respectively. A dot over a symbol indicates the time derivative. We linearize Eqs. (6.22) and (6.23) in terms of the deviations of the physical quantities from their uniform and static values which are indicated by a zero subscript. Assuming that the deviations vary in space and time as $\exp[i(k\cdot r-\omega t)]$, where k is the wave vector and ω is the frequency, we find that the elements of the conductivity tensor have the form

$$\sigma_{\alpha\beta}(\bar{k},\omega) = \frac{in_o q^2}{m\omega}\left[(\delta_{\alpha\beta} - k_\alpha k_\beta)\frac{\omega_d}{\omega_d + i\nu} + \frac{(\omega_d k_\alpha + kV_{o\alpha})(\omega_d k_\beta + kV_{o\beta})}{\omega_d(\omega_d + i\nu) - (k^2 V_F^2/3)}\right], \tag{6.24}$$

where $\omega_d = \omega - k\cdot V_o$, V_F is the Fermi velocity, and k_α is the α-component of the unit vector in the k direction. The dielectric tensor of a semiconductor medium is related to the conductivity tensor by

$$\varepsilon_{\alpha\beta}(\bar{k},\omega) = \varepsilon_\infty \delta_{\alpha\beta} + \frac{4\pi i}{\omega}\sigma_{\alpha\beta}(\bar{k},\omega), \tag{6.25}$$

where ε_∞ is the background dielectric constant.

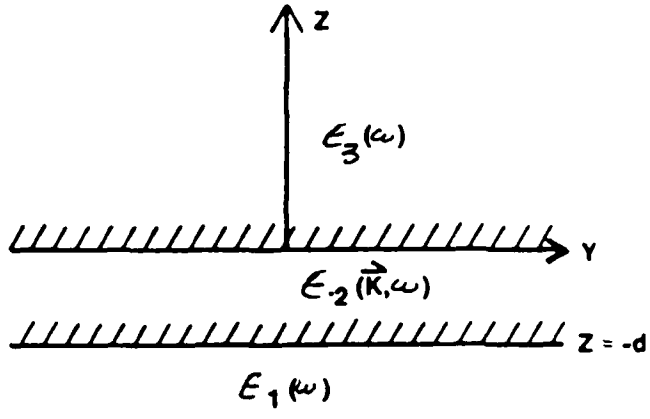

Figure 17. Problem Geometry

Neglecting the thermal pressure gradient term, namely that containing V_F, we have the following components of the dielectric tensor for medium 2:

$$\varepsilon_{YY}(\bar{k},\omega) = \varepsilon_{\infty}^{(2)} \left(1 - \frac{\omega_2^2}{\omega^2} \frac{\omega^2 + V_2^2 k_Z^2}{(\omega - k_y V_Z)^2} \right) \tag{6.26}$$

$$\varepsilon_{YZ}(\bar{k},\omega) = \varepsilon_{zy}(\bar{k},\omega) = -\varepsilon_{\infty}^{(2)} \frac{\omega_2^2}{\omega^2} \frac{k_Z V_Z}{(\omega - k_y V_Z)} \tag{6.27}$$

$$\varepsilon_{ZZ}(\bar{k},\omega) = \varepsilon_{\infty}^{(2)} \left(1 - \frac{\omega_2^2}{\omega^2} \right) \tag{6.28}$$

We can determine the fields in region 2 by assuming that electrons in that region are specularly reflected at the surface. Then we can use the "mirror image" technique and the infinite medium dielectric function, $\varepsilon(Z)$ in region 2(53,54).

The infinite medium is divided into a n layers of thickness d starting from Z = 0. The field at Z = 2nd and are all identical as are the fields at Z = (2n+1)d for n = 0, ± 1, ...

We impose the "mirror-image" conditions

$$\begin{aligned} E_y(nd^+) &= E_y(nd^-) \\ E_y'(nd^+) &= -E_y'(nd^-) \\ E_Z(nd^+) &= -E_Z(nd^-) \\ E_Z'(nd^+) &= E_Z'(nd^-), \end{aligned} \tag{6.29}$$

where the primes denote differentiation with respect to Z. From the Maxwell equation relating E and B, one obtains

$$B_X(nd^+) = -B_X(nd^-). \tag{6.30}$$

The mirror-image conditions lead to discontinuities in E(z) and E'(z) at the surfaces defined above. For surface waves for the geometry stated, one need only consider p-polarization, i.e., the electric field vector lies in the sagittal plane. For this situation, $E_X(z) = 0$.

We define the Fourier transform of E(Z) as

$$-\int_{-\infty}^{\infty} dz \exp(ik_z z) \bar{E}(z) = \bar{E}(k_Z) \tag{6.31}$$

Then the Fourier transform of E'(z) (where the prime indicates differentiation with respect to Z) is

$$FT\{E'(Z)\} = -ik_Z \overline{E}(k_Z) + \sum_{n=-\infty}^{\infty} \Delta \overline{E}(nd) e^{+ik_Z nd} \tag{6.32}$$

In this equation

$$\Delta \overline{E}(nd) = \overline{E}(nd^-) - \overline{E}(nd^+). \tag{6.33}$$

The Fourier transform of E" (z) is

$$FT\{\overline{E}''(z)\} = k_Z^2 \overline{E}(k_Z) + \sum_n \left[\Delta \overline{E}'(nd) - ik_Z \Delta E(nd)\right] e^{+ik_Z nd} \tag{6.34}$$

Using these results, the wave equation describing the electromagnetic fields in region 2 can be Fourier transformed to obtain the matrix equation.

$$\overline{T} \cdot \overline{E} = \overline{A} \tag{6.35}$$

where

$$T_{YY} = \frac{\omega^2}{C^2} \varepsilon_{YY} - k_Z^2, \tag{6.36}$$

$$T_{ZZ} = \frac{\omega^2}{C^2} \varepsilon_{ZZ} - k_Z^2, \tag{6.37}$$

and

$$T_{YZ} = T_{ZY} = \frac{\omega^2}{C^2} \varepsilon_{YZ} + k_Y k_Z \tag{6.38}$$

The quantities E and A are column vectors with components $E_y(k_z)$ and $E_z(k_z)$ and

$$A_Y = \sum_n e^{ik_Z nd} \left[ik_Z \Delta E_Y(nd) - \Delta E_Y'(nd) - ik_Z \Delta E_Z(nd)\right] \tag{6.39}$$

$$A_Z = \sum_n e^{ik_Z nd} \left[-ik_Z \Delta E_Y(nd)\right] \tag{6.40}$$

In the last two expressions, $\Delta E_y(nd) = 0$ and, notice that

$$+ik_Y E_Z + E_Y = \frac{i\omega}{c} B_X \tag{6.41}$$

we have

$$ik_Y \Delta E_Z(nd) + \Delta E_Y(nd) = \Delta \frac{i\omega}{c} B_X(nd) \tag{6.42}$$

Consequently Equations (6.39) and (6.40) reduce to

$$A_Y = -\frac{i\omega}{c} \sum_n e^{ik_Z nd} \Delta B_X(nd) \tag{6.43}$$

and

$$A_Z = 0 \tag{6.44}$$

Now we can use the following relations

$$B_X(nd) = 2B_X(nd^-) = -2B_X(nd^+) \tag{6.45}$$

and

$$\left.\begin{aligned} B_X(0^\pm) &= B_X(2nd^\pm) \\ B_X(-d^\pm) &= B_X\left[(2n+1)d^\pm\right] \end{aligned}\right\} \text{for all } n \tag{6.46}$$

To rewrite Eq. (6.43) as

$$A_y = -\frac{2i\omega}{c}\left[B_x(0^-) - e^{ik_z d} B_x(-d^+)\right] \sum_n e^{ik_z 2nd} \tag{6.47}$$

The summation over n in Eq. (6.47) will vanish when $2k_Z d$ is a multiple of 2π, causing the sum to diverge. Consequently the sum can be written as a sum of delta functions, namely

$$\sum_n e^{ik_z 2nd} = \frac{\pi}{d} \sum_\ell \delta\left(k_z - \frac{\ell\pi}{d}\right), \tag{6.48}$$

So that Eq. (6.47) becomes

$$A_y = -\frac{i\omega}{cd} \sum_{\ell} \left[B_x(0^-) - (-1)^{\ell} B_x(-d^+) \right] \delta \left(k_z - \frac{\ell\pi}{d} \right) \tag{6.49}$$

The wave equation (Eq. (6.35)) can be solved for E_y giving

$$E_y(k_z) = \frac{T_{zz}}{T_{yy} T_{zz} - T_{yz}^2} A_y(k_z) \tag{6.50}$$

Taking the inverse Fourier transform gives

$$E_Y(z) = \frac{-i\omega}{cd} \sum_{\ell=-\infty}^{\infty} e^{-i\ell\pi z/d} \left[B_x(0^-) - (-1)^{\ell} B_x(-d^+) \right] \left[\frac{T_{zz}}{T_{yy} T_{zz} - T_{yz}^2} \right]_{k_z = \frac{\ell\pi}{d}} \tag{6.51}$$

We now proceed to evaluate this expression and explicitly put in k_z-dependence. Utilizing the definitions of Tij given by Eqns. (6.36) - (6.38) and the dielectric tensor components given by Eqns. (6.26) - (6.28), the square bracketed term of Eq. (6.51) can be written as a function of k_z, namely

$$\frac{T_{zz}}{T_{yy} T_{zz} - T_{yz}^2} = \frac{\beta_3}{\beta_1 + k_z^2 \beta_2} \tag{6.52}$$

where $\beta_3 = T_{zz}$ and

$$\beta_1 = \varepsilon_x^{(2)} \frac{\omega^2}{c^2} \left[\varepsilon_\infty^{(2)} \frac{\omega^2}{c^2} \left(1 - \frac{\omega_2^2}{\omega^2} \right) - k_y^2 \right] \left[1 - \frac{\omega_2^2}{(\omega - k_y V_2)^2} \right] \tag{6.53}$$

$$\beta_2 = -\varepsilon_x^{(2)} \frac{\omega_2^2}{c^2} \frac{V_2^2}{(\omega - k_y V_2)^2} \frac{\omega^2}{c^2} \varepsilon_x^{(2)} \left(1 - \frac{\omega_2^2}{\omega^2} \right)$$

$$+ \frac{\varepsilon_x^{(2)} \omega^2}{c^2} \left(\frac{\omega_2^2}{(\omega - k_y V_2)^2} - 1 \right) - \left[\varepsilon_x^{(2)} \right]^2 \frac{\omega_2^4}{c^4} \frac{V_2^2}{(\omega - k_y V_2)^2} \tag{6.54}$$

Equation (6.51) can now be written as

$$\frac{icd}{\omega} E_y(0^-) = B_x(0^-) \sum_{\ell} \frac{\beta_3}{\beta_1 + k_z^2 \beta_2} - B_x(-d^+) \sum_{\ell} \frac{(-1)^{\ell} \beta_3}{\beta_1 + k_z^2 \beta_2} \tag{6.55}$$

In addition we can write

$$\frac{icd}{\omega} E_y(-d^+) = B_x(0^-) \sum_{\ell} \frac{(-1)^{\ell} \beta_3}{\beta_1 + k_z^2 \beta_2} - B_x(-d^+) \sum_{\ell} \frac{\beta_3}{\beta_1 + k_z^2 \beta_2} \tag{6.56}$$

In Eqs. (6.55) and (6.56) remember that $k_z = \ell\pi/d$.

Thus consider the sum

$$S_m = \sum_{\ell} \frac{\frac{d^2}{\pi^2 \beta_2} \beta_3 (-1)^{\ell m}}{\frac{d^2 \beta_1}{\pi^2 \beta_2} + \ell^2} \tag{6.57}$$

$$S_1 = \frac{d\beta_3}{\sqrt{\beta_1 \beta_2}} \operatorname{cosech}\left(d\sqrt{\frac{\beta_1}{\beta_2}} \right) \tag{6.58}$$

$$S_2 = \frac{d\beta_3}{\sqrt{\beta_1 \beta_2}} \coth\left(d\sqrt{\frac{\beta_1}{\beta_2}} \right) \tag{6.59}$$

From these results, Eqs. (6.55) and (6.56) can be written as

$$E_y(0^-) = B_x(0^-) \Upsilon_2 - B_x(-d^+) \Upsilon_1 \tag{6.60}$$

$$E_y(-d^+) = B_x(0^-) \Upsilon_1 - B_x(-d^+) \Upsilon_2, \tag{6.61}$$

where

$$\Upsilon_1 = \frac{-i\omega}{c} \frac{\beta_3}{\sqrt{\beta_1 \beta_2}} \operatorname{cosech}\left(d\sqrt{\frac{\beta_1}{\beta_2}} \right) \tag{6.62}$$

$$\gamma_2 = \frac{-i\omega}{c} \frac{\beta_3}{\sqrt{\beta_1\beta_2}} \coth\left(d\sqrt{\frac{\beta_1}{\beta_2}}\right) \tag{6.63}$$

Next the boundary conditions are considered.

Region 1 ($z \geq 0$)

$$\frac{E_y(-d^-)}{B_x(-d^-)} = \frac{-i\alpha_1 c}{\omega\varepsilon_1}, \tag{6.64}$$

where

$$\alpha_1^2 = k_y^2 - \varepsilon_1 \frac{\omega^2}{c^2} \tag{6.65}$$

Region 2 ($0 < z \leq -d$)

The fields for this region are given by Eqs. (6.60) and (6.61).

Region 3 ($z \leq -d$)

$$\frac{E_y(0^+)}{B_x(0^+)} = \frac{-i\alpha_3 c}{\omega\varepsilon_3}, \tag{6.66}$$

where

$$\alpha_3^2 = k_y^2 - \varepsilon_3 \frac{\omega^2}{c^2} \tag{6.67}$$

From Eq. (6.61)

$$\frac{E_y(-d^+)}{B_x(-d^+)} = \gamma_1 \frac{B_x(0^-)}{B_x(-d^+)} - \gamma_2 = \frac{-i\alpha_1 c}{\omega\varepsilon_1}, \tag{6.68}$$

From Eq. (6.60)

$$\frac{E_y(0^-)}{B_x(0^-)} = \gamma_2 - \frac{B_x(-L^+)}{B_x(0^-)} - \gamma_1 = \frac{-i\gamma_3 c}{\omega\varepsilon_3}, \tag{6.69}$$

From these expressions one can obtain the following dispersion relation:

$$\left(\gamma_2 - \frac{i\alpha_1 c}{\omega\varepsilon_1}\right)\left(\gamma_2 - \frac{i\alpha_3 c}{\omega\varepsilon_3}\right) = \gamma_1^2 \tag{6.70}$$

In this expression we take the dielectric functions of medium 1 and 3 to be, respectively,

$$\varepsilon_1 = \varepsilon_\infty^{(1)} + \frac{4\pi i\sigma_1}{\omega} \tag{6.71}$$

$$\varepsilon_3 = \varepsilon_\infty^{(3)} + \frac{4\pi i\sigma_3}{\omega}, \tag{6.72}$$

where $\sigma_{1,3}$ are the conductivities.

In the non-retarded limit, i.e., $c \to \infty$, the dispersion relation given by Eq. (6.70) can be written as

$$\Gamma_1\Gamma_2 - \Gamma_3\Gamma_4 \exp\left(\frac{V_2 k_y}{\omega_2} \cdot \frac{\omega_2 d}{V_2}\right) = 0, \tag{6.73}$$

where

$$\Gamma_1 = \varepsilon_\infty^{(2)}\left[\left(\frac{\omega}{\omega_2} - \frac{V_2 k_y}{\omega_2}\right)^2 - 1\right] + \varepsilon_1\left(\frac{\omega}{\omega_2} - \frac{V_2 k_y}{\omega_2}\right)^2 \tag{6.74}$$

$$\Gamma_2 = \varepsilon_\infty^{(2)}\left[\left(\frac{\omega}{\omega_2} - \frac{V_2 k_y}{\omega_2}\right)^2 - 1\right] + \varepsilon_3\left(\frac{\omega}{\omega_2} - \frac{V_2 k_y}{\omega_2}\right)^2 \tag{6.75}$$

$$\Gamma_3 = \varepsilon_\infty^{(2)}\left[\left(\frac{\omega}{\omega_2} - \frac{V_2 k_y}{\omega_2}\right)^2 - 1\right] - \varepsilon_1\left(\frac{\omega}{\omega_2} - \frac{V_2 k_y}{\omega_2}\right)^2 \tag{6.76}$$

$$\Gamma_4 = \varepsilon_\infty^{(2)}\left[\left(\frac{\omega}{\omega_2} - \frac{V_2 k_y}{\omega_2}\right)^2 - 1\right] - \varepsilon_3\left(\frac{\omega}{\omega_2} - \frac{V_2 k_y}{\omega_2}\right)^2 \tag{6.77}$$

6.2.3 Results and Discussion

Equation (6.73) was solved numerically for ω as a function of wave vector k_y, i.e., real values of k_y were input and complex values of ω were calculated.

Thus we have a theoretical model for the HEMT structure (Fig. 1) as a three-layer system where the middle layer is the electron channel. The adjacent layers can be modeled as undoped GaAs and doped AlGaAs (partially depleated). One can vary the conductivities of the adjacent layers as desired and note the consequent effect on SCW amplification. Preliminary results indicate convective instabilities (amplification) when the adjacent media conductivies are as follows:

$$\sigma_1 = \sigma_3 \neq 0$$

$$\sigma_1 \neq \sigma_3 \neq 0$$

$$\sigma_1 = o, \sigma_3 \neq 0$$

An obvious and necessary extension of this theory is to include optical phonons. This is in progress.

VII. CONCLUSIONS

Both experimental and theoretical work has been done on the feasibility of a device, based on utilizing the GaAs/AlGaAs HEMT structure, for amplifying microwaves. The accomplishments are as follows.

A number of design considerations baring on concept feasibility were investigated. These include HEMT channel carrier concentration, carrier scattering, including the creation of LO phonons, penetration depth of microwaves into the HEMT structure, etc. Based on these considerations and other work, the concept appears feasible. The major amplifier loss mechanisms, apart from the slow-wave circuit losses, would be the creation of LO optical phonons and, possibly, Landau damping. The latter has not been investigated, but would be a suitable topic for future work.

During the first part of the program, fabrication techniques were developed for interdigital slow-wave circuits and ohmic contacts on HEMT structures. Several prototype devices were successfully fabricated and two were successfully tested. The microwave tests indicate that microwaves can be coupled to the drifting HEMT channel electrons. An interesting point is that interdigital electrode can be used as a gate and hence determine the HEMT channel electron concentration. This is important because the maximum slow SCW gain occurs at the plasma frequency, which of course, is a function of the electron concentration. Thus it appears that one could use the interdigital electrode/gate bias to select the frequency one wants amplified. The frequency must be one compatible with the slow-wave circuit, however.

Theoretical work on doped GaAs shows that the TO phonons behave as the "resistive wall" required for electromagnetic wave amplification. In addition, a theoretical investigation is in progress on the interaction of electromagnetic waves and drifting electrons in HEMT structures. Consistent with what has been observed above, amplifying instabilities are in evidence.

In conclusion, the device concept for microwave amplification appears valid, however, experimental feasibility has yet to be demonstrated. It may be that the various losses would preclude microwave amplification. This point remains unresolved at this time.

VIII. TECHNICAL PAPERS RESULTING FROM THIS WORK

1. B. G. Martin and R. F. Wallis, "Theory of the Interaction of Optical Phonons with Space Charge Waves in Solid State Plasmas", Bull. Am. Phys. Soc. 32, 451 (1987).

2. B. G. Martin and R. F. Wallis, "Theory of the Interaction of Electromagnetic Waves and Drifting Electrons in Modulation --Doped AlGaAs/GaAs Heterestructures", paper to be presented at the March 1988 A.P.S. Meeting in New Orleans, Louisiana.

IX. REFERENCES

1. G. A. Baraff and S. J. Buchsbaum, Phys. Rev. 144, 255 (1966).

2. G. S. Kino, Appl. Phys. Letters 12, 312 (1965).

3. B. E. Burke and G. S. Kino, Appl. Phys. Letters 12, 310 (1968).

4. S. l. Khankina and V. M. Yakovenko, Sov. Phys. - Solid State 9, 2313 (1968).

5. A. Bers and B. E. Burke, Appl. Phys. Letters 16, 300 (1970).

6. B. G. Martin, A. A. Maradudin, and R. F. Wallis, Surf. Sci. 19 37 (1980).

7. B. G. Martin, J. J. Quinn, and R. F. Wallis, Proceedings of the 4th Int. Conf. on Solid Surfaces, Cannes, France (1950).

8. B. G. Martin, J. J. Quinn, and R. F. Wallis, Surf. Sci. 105, 145 (1981).

9. Juras Pozhela, Plasma and Current Instabilities in Semiconductors, Pergamon Press (1981).

10. C. K. Birdsall, G. R. Brewer, and A. V. Haeff, Proc. I.R.E. 41, 865 (1953).

11. C. K. Birdsall and J. R. Whinney, J. Appl. Phys. 24, 1072 (1965).

12. Akira Hasegawa, J. Phys. Soc. Japan 20 1072 (1965).

13. S. l. Khankina and V. M. Yakovenko, Sov. Phys. - Solid State 9, 443 (1967).

14. Yoshihiko Mizushima and Tsuneta Sudo, IEEE Trans. Electron Devices ED-17, 541 (1970).

15. Martin C. Steele and Bayram Vural, Wave Interactions in Solid State Plasmas, McGraw-Hill (1969).

16. L. Solymar and E. A. Ash, Int. J. Electronics 20 127 (1966).

17. Masao Sumi, Jap. J. Appl. Phys. 6, 688 (1967).

18. S. Lefeuvre and V. Fouad Hanna, Int. J. Electronics 35 145 (1973).

19. Avraham Gover and Amnon Yariv, J. Appl. Phys. 45, 2596 (1974).

20. J. Thiennot, J. Appl. Phys. 46 3925 (1975).

21. Henri Baudrand, Tanos El Khoury, and Desire Lilonga, IEEE Trans. Microwave Theory and Techniques MTT-32, 1434 (1954).

22. Frank Crowne, J. Appl. Phys. 57, 4772 (1985).

23. A. H. W. Beck, Space Charge Waves and Slow Electromagnetic Waves, Pergammon Press (1958).

24. J. R. Fierce, Almost All About Waves, the MIT Press (1974).

25. L. J. Chu, paper presented at the Institute of Radio Engineers Electron Devices Conference, University of New Hampshire, June, 1951.

26. Andrew V. Haeff, Proceedings of the I.R.E. 37 4 (1949).

27. J. R. Fierce and W. B. Hebenstreit, Bell Syst. Tech. J. 28, 33 (1949).

28. A. V. Hollenberg, Bell Syst. Tech. J. 28, 52 (1949).

29. B. G. Martin and R. F. Wallis, "Theory of Dispersion Instabilities Associated With Surface Electromagmetic Waves in Layered Semiconductor Media," paper accepted for publication in Phys. Rev. B.

30. K. L. Kliewer and R. Fuchs, Phys. Rev. 172, 605 (1968).

31. P. A. Sturrock, Phys. Rev. 112, 1458 (1958).

32. T. J. Drummond, W. Kopp, H. Morkoc, and M. Keever, Appl. Phys. Lett. 41, 277 (1982).

33. P. J. Price, Annals of Physics 133, 217 (1981).

34. T. J. Drummond, M. Keever, and H. Morkoc, Jap. J. Appl. Phys. Lett. 21, L65 (1982).

35. K. Hirakawa, H. Sakaki, and J. Yoshino, Appl. Phys. Lett. 45, 253 (1984).

36. G. Weimann and W. Schlapp, Appl. Phys. Lett. 46, 411 (1985).

37. Kotaro Tsubaki, Akira Sugimura, and Kenji Kumabe, "Electron Mobility Limits of Two-Dimensional Electron Gas in N-AlGaAs/GaAs at Low Temperature," to appear in J. Appl. Phys.

38. M. E. Hines, IEEE Trans. Electron Devices ED-16, 88 (1969).

39. Karl Hess, IEEE Trans. Electron Devices ED-28, 937 (1981).

40. Timothy J. Maloney, IEEE Electron Device Letters EDL-1, 54 (1980).

41. Gordon S. Kino, IEEE Trans. Electron Devices ED-17, 178 (1970).

42. C. K. Birdsall, Tech. Rpt. No. 36, Elec. Res. Lab., Stanford Univ., Palo Alto, CA.

43. J. R. Pierce, Proc. I.R.E. 37 980 (1949).

44. Jasprit Singh and K. K. Bajaj, Bull. Am. Phys. Soc. 29, 234 (1984).

45. T.J.B. Swanenburg, IEEE Trans. Electron Devices ED-20, 630 (1973).

46. Masao Sumi and Toshimasa Suzuki, Appl. Phys. Lett. 13, 326 (1968).

47. B. G. Martin and R. F. Wallis, Bull. Am. Phys. Soc. 32, 451 (1987).

48. See references listed in the following: B. G. Martin and R. F. Wallis, Phys. Rev. B 32, 3824 (1985).

49. T. Tajima and S. Ushioda, Phys. Rev. B 18, 1892 (1978).

50. B. G. Martin, A. A. Maradudin, and R. F. Wallis, Surface Sci. 91, 37 (1980).

51. J. S. Blakemore, J. Appl. Phys. 53, R123 (1982).

52. R. N. Sudan, Phys. Fluids 8, 1899 (1965).

53. R. F. Wallis, D. Castiel, and J. J. Quinn, in Proceedings of the 1978 Conference on the Physics of Semiconductors, Inst. Phys. Cont. Ser. No. 43, p. 203 (1979).

54. A. Equiluz and J. J. Quinn, Phys. Rev. B 14, 1347 (1976).

END
DATE
FILMED
7-88
DTIC